Development of Biofunctionalized Nanocomposite Based Biosensor for Oral Cancer Detection

to be submitted as Major Project in partial fulfillment of the requirement for the degree of

M. Tech. (Biomedical Engineering)

Submitted by

Niharika Gupta

(Roll No. 2K14/BME/13)

Delhi Technological University

Under the supervision of

Prof. Bansi D. Malhotra

Department of Biotechnology

Delhi Technological University, Delhi 110042, India

DECLARATION

I, **Niharika Gupta**, hereby declare that the dissertation entitled **'Development of Biofunctionalized Nanocomposite Based Biosensor for Oral Cancer Detection'** submitted is in partial fulfillment of the requirement for the award of the degree of Master of Technology in Biomedical Engineering, Delhi Technological University. It is a record of original and independent research work done by me under the supervision and guidance of **Prof. Bansi. D. Malhotra**, Department of Biotechnology, Delhi Technological University, Delhi. The information and data enclosed in the dissertation is original and has not formed the basis of the award of any Degree/Diploma/Fellowship or other similar title to any candidate of the University/Institution.

Date:

Niharika Gupta
Roll No.: 2K14/BME/13
M. Tech. (Biomedical Engineering)
Department of Biotechnology
Delhi Technological University
Shahbad Daulatpur,
Main Bawana Road, Delhi 110042, INDIA

Delhi Technological University

Certificate

This is to certify that the dissertation entitled **‘Development of Biofunctionalized Nanocomposite Based Biosensor for Oral Cancer Detection’** submitted by **Niharika Gupta (2K14/BME/13)** is in the partial fulfillment of the requirements for the reward of the degree of Master of Technology, Delhi Technological University, Delhi, is an authentic record of the candidate’s own work carried out by her under my guidance. The information and data enclosed in this thesis is original and has not been submitted elsewhere for honoring of any other degree.

Prof. D. Kumar
Head
Department of Biotechnology
Delhi Technological University

Prof. Bansi D. Malhotra
(Project Mentor)
Department of Biotechnology
Delhi Technological University

Acknowledgement

I wish to express my profound sense of gratitude to my mentor **Prof. Bansi D. Malhotra**, Department of Biotechnology, Delhi Technological University for his valuable guidance, much sought-after suggestions and encouragement throughout these investigations. I heartily thank **Prof. D. Kumar**, Head, Department of Biotechnology, Delhi Technological University, for his kind support and help in providing all facilities in a timely manner.

I am highly indebted to **Ms. Shine Augustine**, **Mr. Suveen Kumar** and **Mr. Saurabh Kumar** (Research Scholars) whose guidance and constant supervision helped me decide on my project work and complete it in a timely manner. I greatly acknowledge **Dr. C. M. Pandey,** DST-INSPIRE Faculty, Department of Applied Chemistry, Delhi Technological University, who supported me in every possible way to complete the project work.

I thank all the faculty members of Department of Biotechnology, Delhi Technological University for providing me with valuable suggestions and all necessary facilities required to complete this project work. I also thank **Mr. Chhail Bihari Singh**, **Mr. Jitender Kumar** and all other non-teaching staff of Department of Biotechnology, Delhi Technological University for aiding me in finding requirements for the project work.

I thank my fellow colleagues **Ashish**, **Shweta Panwar**, **Divya Rani Dubey**, **Anindita Sen** and **Md. Umar** for assisting me when in need and encouraging me to carry out this work.

Lastly, this report would not have been possible if not for the patience and encouragement of my family. I thank my parents for their support throughout the framing of this report.

Niharika Gupta

2K14/BME/13

List of abbreviations

0-D	Zero-dimensional
1-D	One-dimensional
2-D	Two-dimensional
3-D	Three-dimensional
ΔE_p	Peak potential difference
μA	Microampere
μg	Microgram
APTES	3-(Aminopropyl)-triethoxysilane
AgCl	Silver chloride
BSA	Bovine serum albumin
CA15.3	Cancer antigen 15.3
CEA	Carcinoembryogenic antigen
CNTs	Carbon nanotubes
CV	Cyclic voltammetry
DNA	Deoxyribonucleic acid
DPV	Differential pulse voltammetry
EDC	N-ethylene-N’-(3-dimethylaminopropyl) carbodiimide
ELISA	Enzyme-linked immunosorbent assay
E_{pa}	Anodic peak potential
E_{pc}	Cathodic peak potential
FT-IR	Fourier transform infrared spectroscopy
IL-1	Interleukin 1
IL-6	Interleukin 6
IL-8	Interleukin 8
IGF	Insulin growth factor
I_{pa}	Anodic peak current
I_{pc}	Cathodic peak current
ISO	International Organization for Standardization
ITO	Indium-tin- oxide
JCPDS	Joint Committee on Powder Diffraction Standards

LOD	Limit of detection
miRNA	Micro-ribonucleic acid
mL	Millilitre
mM	Millimolar
ng	Nanogram
NHS	N-hydroxysuccinimide
nMOx	Nanostructured metal oxides
NNAL	4-(methylnitrosamino)-1-(3-pyridyl)-1-butanol
NNK	4-(methylnitrosamino)-1-(3-pyridyl)-1-butanone
nY_2O_3	Nanostructured yttria
$nZrO_2$	Nanostructured zirconia
ORAOV	Oral cancer associated
OSCC	Oral squamous cell carcinoma
PBS	Phosphate buffered saline
POC	Point-of-care
rGO	Reduced graphene oxide
RNA	Ribonucleic acid
RSD	Relative standard deviation
SEM	Scanning electron microscopy
SOFC	Solid oxide fuel cells
TNF	Tumor necrosis factor
VEGF	Vascular endothelial growth factor
WHO	World Health Organization
XRD	X-ray diffraction
YSZ	Yttria-stabilized zirconia

List of Figures

List of Tables

Table of Contents

Development of Biofunctionalized Nanocomposite Based Biosensor for Oral Cancer Detection

Niharika Gupta

Delhi Technological University, New Delhi

e-mail ID: niharika.gupta990@gmail.com

Abstract

This dissertation deals with the results of studies relating to the fabrication of a novel biosensing platform based on yttria stabilized zirconia decorated reduced graphene oxide (nY_2O_3-$nZrO_2$-rGO) nanocomposite, for sensitive label-free detection of oral cancer biomarker CYFRA-21-1. One step, hydrothermal method has been used to synthesize nY_2O_3-$nZrO_2$-rGO nanocomposite and 3-aminopropyl triethoxysilane (APTES) has been utilized for functionalization of the synthesized nY_2O_3-$nZrO_2$-rGO nanocomposite. Thin films of the APTES/nY_2O_3-$nZrO_2$-rGO nanocomposite have been obtained onto ITO electrodes via electrophoretic deposition (45 V; 180 s). Monoclonal anti-CYFRA-21-1 antibodies immobilized on to this APTES/nY_2O_3-$nZrO_2$-rGO/ITO platform via EDC-NHS mediated covalent conjugation and BSA was used for blocking of non-specific sites yielding the BSA/anti-CYFRA-21-1/APTES/nY_2O_3-$nZrO_2$-rGO/ITO immunoelectrode. Structural, morphological and electrochemical characterization of the synthesized nanocomposite and the fabricated electrodes was conducted via X-ray diffraction (XRD), scanning electron microscopy (SEM), Fourier transform infrared (FT-IR) spectroscopy, differential pulse voltammetry (DPV) and cyclic voltammetry (CV). Electrochemical response studies revealed that the proposed immunosensor can efficiently detect CYFRA-21-1 in a wide linear detection range of 0.25-22 ng mL^{-1} with excellent sensitivity of 9.6 µA mL $ng^{-1}cm^{-2}$ and detection limit of 0.1 ng mL^{-1}.

Chapter 1

Introduction

1. Introduction

"We'll have more power in the volume of a sugar cube than exists in the entire world"

\- *Ralph Merkle*

The above statement just about sums up the potential of nano-inspired materials and the vast array of applications they can be used in. The research into nanomaterials has been expanding for about 5 decades owing to their unique properties that can be tailored without bringing a change in their chemical structure. The high surface-to-volume ratio provides nanomaterials with high surface reactivity and thus, makes them suitable for a range of applications, including catalysis, miniaturized electronic chips, light-weight materials, molecular diagnostics, targeted delivery, etc. Over the years, different classes of nanomaterials have emerged depending on the type of their chemical structure, such as metallic nanoparticles, polymeric nanomaterials, carbon based materials, etc. However, certain inherent limitations of single phase nanomaterials have restricted their large-scale applications such as high surface reactivity, instability in aqueous solutions, agglomeration, etc. This problem has been resolved, to some extent by the introduction of nanocomposite materials.

Nanocomposites are a special class of materials consisting of two or more phases, with at least one of the phases in the nano length scale. They display synergistically enhanced mechanical, optical, electrochemical and thermal properties and thus, offer the possibilities of developing novel composite materials with properties which do not exist naturally. Ceramic-based nanocomposites have been the subject of research in the past many years due to their superior mechanical and electrical properties. Particularly, yttria-stabilized zirconia (YSZ) has gained attention owing to its exceptional properties, such as super plasticity at low temperatures, high electrical and ionic conductivity, high toughness, non-toxicity, etc. These superior properties have rendered YSZ useful in a number of applications, including implantable devices, dental fillers, solid oxide fuel cells, gas sensors, etc. Carbon-based nanomaterials, particularly reduced graphene oxide (rGO), have also gained attention in the development of nanocomposites. They bring several advantageous properties to the nanocomposite materials, such as exceptional conductivity, high electrocatalytical rate, increased mechanical strength and improved thermal and tribological properties. Particularly, composites of rGO with nanostructured ZrO_2 ($nZrO_2$) have emerged as novel materials with exceptional tunable properties. They possess high mechanical strength and electrical conductivity. Likewise, rGO addition may also enhance the properties of YSZ composites. However, efforts are needed to further characterize YSZ-rGO nanocomposites which would lead to the full realization of their potential applications.

rGO-$nZrO_2$ nanocomposites have found many applications ranging from nanofoams for oil adsorption to biomedical implants. One of the emerging, and perhaps the most significant, applications of rGO-$nZrO_2$ is the development of biosensors. A biosensor is an analytical device which integrates a biorecognition element with a physicochemical transducer, allowing the quantitative detection of a chemical or a biological analyte. Of particular importance are electrochemical biosensors which are currently at the crux of the point-of-care health care. Nanomaterial-enabled electrochemical biosensors possess enhanced sensitivity, higher signal transduction rate and improved signal-to- noise ratio. Thus, nanomaterials seem to have become an integral part of biosensor fabrication. Given the fact that nanocomposites exhibit synergistic enhancement in properties, YSZ-rGO could prove as a potential candidate for biosensor development.

Cancer diagnosis is one of the most prominently researched applications for biosensors. Sensitive detection of cancer-related analytes in body fluids has been the focus of biosensing technology for a long time now. Particularly, biosensors for oral cancer diagnosis have gained attention from various research groups in the recent past. Oral cancer comprises of malignant transformation in the mouth, lips, pharangyeal regions, tongue, and other parts of the oral cavity. Epidemiological surveys by WHO have found that the prevalence of oral cancer is the highest among South Asians with India being the oral cancer capital in the world. Several risk factors have been cited for the high occurrence of oral cancer in developing regions, including chewing tobacco and betel quid, alcoholism, smoking, poor nutrition and dental hygiene, genetic factors, etc. In most cases, the symptoms of oral cancer which include white or red patches, difficulty in swallowing, wounds that do not heal, etc., are often ignored and hence the disease has a high mortality rate owing to diagnosis in later stages. Biopsy is currently the most prominent technique for the diagnosis for oral cancer. However, other tests such as toluidine blue dye assay, chemilumenescence, and other visual aids are often conducted along with biopsy. These techniques possess a number of disadvantages, such as high invasiveness, subjective interpretation, discomfort to patient, high costs, etc. This has called for the development of reliable diagnostic techniques for oral cancer detection.

Advancements in the techniques of proteomics and genomics have led to the discovery of a wide array of biomolecules whose concentrations in various body fluids, including serum, saliva, urine, etc., strongly correlate to the presence of oral cancer. Such analytes are referred to as biomarkers. Furthermore, recent findings have suggested that saliva can efficiently act as a diagnostic medium for oral cancer detection owing to the inherent advantages it offers, such as non-invasive nature, easy sample processing, low costs for storage and transportation, etc.

Extensive literature is now available describing the various types of potential salivary markers, such as VEGF, CYFRA-21-1, p53, IL-6, etc. and their role in oral cancer detection. Out of these, CYFRA-21-1, a fragment of cytokeratin-19, has emerged as a promising salivary biomarker for oral cancer. Its concentration in saliva increases several folds in oral cancer and can be utilized for monitoring as well. The current conventional assays are unable to detect low concentrations of biomarkers, including ELISA. This limitation can be overcome, to a large extent, by the development of ultrasensitive biosensors for oral cancer detection. Several reports have confirmed that nanomaterials-enhanced biosensing platforms can be efficiently utilized to detect oral cancer biomarkers. However, more efforts are needed to develop a sensitive biosensing platform for clinical detection of oral cancer.

This report describes results of the studies relating to fabrication of a functionalized Y_2O_3-ZrO_2-rGO based biosensing platform for sensitive detection of CYFRA-21-1, an oral cancer biomarker. Efforts have been made to characterize the structural, morphological and electrochemical characteristics of the synthesized nanocomposite and the fabricated electrodes. Differential pulse voltammetry (DPV) has been utilized for measuring the response of the biosensing platform towards CYFRA-21-1 antigen. To the best of our knowledge, this is the first report on the use of Y_2O_3-ZrO_2-rGO nanocomposite as a biosensing platform.

Chapter 2

Literature Review

2. Literature Review

2.1 Nanomaterials

Since the radical views of Richard Feynman on the possibility of writing an entire encyclopedia on the head of a pin were first made public in 1959, the world has come a long way in its quest to control materials at the nano-scale (Feynman 1960). Nanomaterials as they are referred to now, comprise of a special class of materials that have at least one of their dimensions below 100 nm, wherein 1 nm is equal to one billionth of a metre or roughly half the width of a human hair. There has been a lot of excitement on the preparation and possible applications of nanomaterials in the recent past owing to the exceptional properties that they exhibit. For example, the same aluminum foil which is used for food wrapping gets transformed into a lightweight rocket fuel when broken down into nanoparticles (Meda et al. 2007). However, the existence of nanomaterials is much older than one might think, as they are not merely the end result of the human imagination. Nature has been engineering nanomaterials since millions of years ago. Right from halloysite clay nanotubes to carbon fullerenes in volcanic ash to shells and bones in living organisms, the complexity of naturally occurring nanomaterials has perplexed mankind since long and inspired to create what are today known as “engineered nanomaterials.”

The leading advantage of these engineered nanomaterials is the large surface area/volume ratio, which translates to a very high surface reactivity with the surrounding surface. This exceptional property is what makes metal nanoparticles, such as Pt, Pd, Au, Ag, etc. an ideal candidate for catalysis or sensor applications (Doria et al. 2012; Wu and Zheng 2013). Another distinctive feature that appears due to change in surface properties is the improvement in mechanical properties in relation to the same bulk materials. Another interesting phenomenon which comes into play when size reaches the atomic domain is the quantum confinement effect which gives rise to unusual size-dependent electrical and optical properties (Moody 2013; Zhao et al. 2004). Further, since biological systems comprise of nanoscale materials (e.g., proteins, DNA, etc.), nanomaterials can be utilized for use in artificial components within the cells to diagnose/fight diseases, illnesses, viruses, and other superficial weaknesses (e.g., artificial muscles) (Fan et al. 2012; Wang et al. 2011). Another key benefit of the nanomaterials is the ability to tailor their fundamental properties (e.g., electronic properties, magnetization, optical properties (color), melting point, hardness, etc.) without a change in their chemical composition. This allows for the fabrication of miniaturized devices comprising of nanomaterials with properties most suitable to the desired application (Erdem 2007; Sun et al. 2014; Walt 2005).

2.1.1 Types of nanomaterials

Different classes of nanomaterials have emerged over the years depending on their chemical structure, dimensionality or particular surface morphology. There are four primary types of nanomaterials based on dimensionality:

(i) 0-D (e.g., nanoparticles, nanoclusters, nanocrystals): These materials have diameters <100 nm, and are denoted by nanoparticles, nanoclusters, or nanocrystals.

(ii) 1-D (e.g., nanotubes, nanofibers, nanowires): These materials display predominant growth in only one dimension (such as, length), e.g., nanowires, nanotubes, etc.

(iii) 2-D (nanosheets, layers): These materials tend to occur in sheets with thickness in the atomic length scale, e.g., graphene

(iv) 3-D (nanofoams, etc.): These materials are composed by aligning 2-D and 1-D materials in different arrangements, e.g., 3-D nanowire arrays, graphene nanofoams, etc.

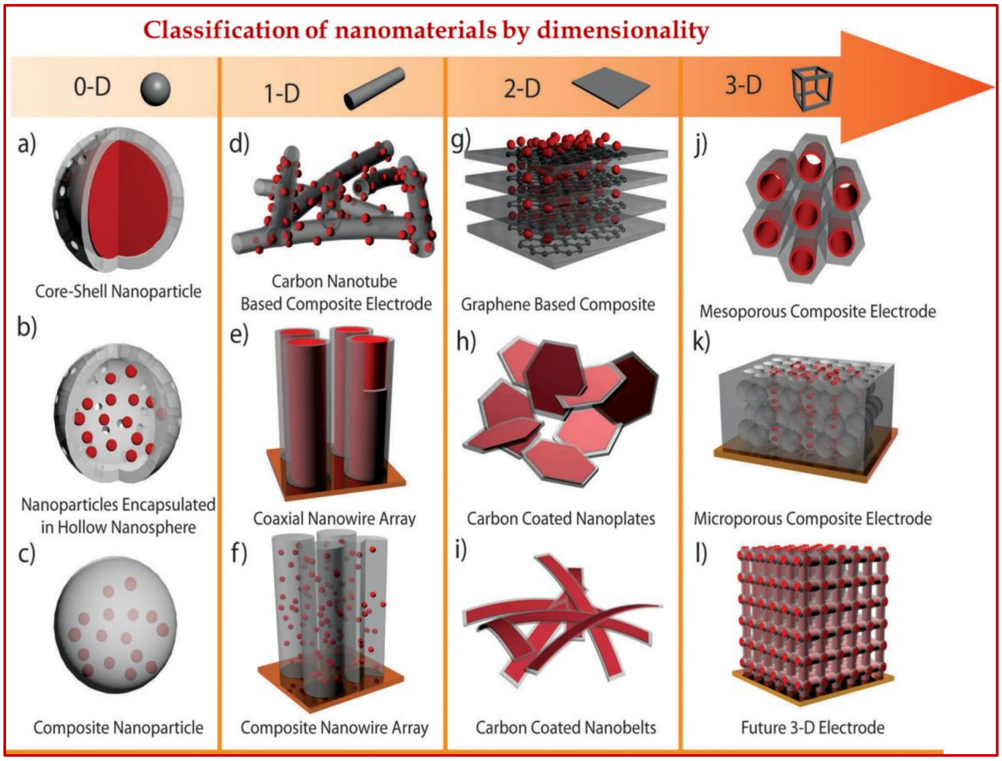

Figure 2.1 Classification of nanomaterials on the basis of dimensionality

On the basis of chemical structure, most nanomaterials can be classified into four types:

- Polymeric nanomaterials
- Carbon based nanomaterials
- Metallic nanomaterials
- Nanocomposites

The polymeric nanomaterials are polymers built from nanosized monomeric units. The surface of these polymers possesses numerous chain ends, which can be tailored accordingly to perform specific chemical functions. Also, many polymeric nanomaterials possess internal cavities in which other small sized molecules can be encapsulated. This property has been utilized in targeted drug delivery and *in vivo* diagnostics (Muhamad12 et al. 2014). Carbon based nanomaterials are composed mostly of carbon and take form in a variety of shapes and morphologies, such as hollow spheres (fullerenes), tubes (carbon nanotubes), sheets (graphene), etc. Most of these nanomaterials possess exceptional electrocatalytical activity owing to their high electron transfer rate (Shao et al. 2010). Thus, carbon-based nanomaterials, particularly graphene, have found wide applications in the development of new generation electrochemical devices such as supercapacitors, batteries, sensing, photocatalysts, etc. Moreover, the large surface area and fairly good biocompatibility render them ideal for applications in targeted delivery and *in vivo* diagnostics. Metallic nanoparticles include noble metals, such as nanogold, nanosilver, etc., quantum dots and nanostructured metal oxides such as TiO_2, MnO, MgO, etc. The unique tailorable magnetic, optical and electrical properties of metallic nanoparticles have found them a number of applications, such as biomedical imaging, theranostics, etc. (Chang et al., 2013, Zhu et al., 2014). In addition to having a large surface area, they possess surface hydroxyl groups, which not only enables high loading of biomolecules but also allows easy functionalization via different conjugation strategies (Kumar et al., 2016). Nanocomposites are a special class of nanomaterials comprising of nanoparticles conjugated with other types of nanoparticles, such as rGO-ZrO_2, Ag@CNT, Pt-rGO, etc. Nanocomposites display synergistic enhancement in the mechanical, optical, or/and electrical properties in relation to the constituting nanomaterials (Kumar et al., 2016; Ali et al., 2015). For instance, a nanocomposite consisting of Pt and rGO displays synergistic improvement in both the electron transfer rate and catalytic properties (Solanki et al., 2013).

2.1.2 Limitations of Nanomaterials

Despite widespread applications of nanomaterials, they have not yet been fully exploited for many commercial applications owing to a number of inherent limitations. As discussed earlier, nanomaterials possess high surface to volume ratio resulting in high surface energy. This ultimately translates to high vulnerability of nanomaterials towards agglomeration particularly when they are synthesized in solution. Many times, the charge repulsion among the grains is superseded by the drastic increase in surface energy leading to formation of more stable, bigger particles. The presence of impurities and other by-products may also enhance the rate of agglomeration. Thus, it is very difficult to control the size and morphology of nanomaterials. Further, since nanoparticles are thermodynamically unstable, they are more prone to undergo transformation which can have a deleterious effect on their properties. A common solution to this problem has been the encapsulation of nanomaterials in another bigger/non-reacting matrix or material (e.g., a surfactant). Such encapsulation surely reduces agglomeration but only at the expense of some of the properties of nanomaterials.

An alternative to this strategy could be the conjugation of two or more different types of nanomaterials to form a nanocomposite, such that there is a synergistic enhancement in each of their properties. For instance, conjugation of rGO with other nanomaterials such as nMOx, increases the interatomic distance between individual rGO sheets leading to enhanced electron transfer rate. At the same time, the grafting of nMOx on rGO sheets prevents the agglomeration of of nMOx particles (Kumar et al., 2016a; 2015b; Singh et al., 2012). Thus, nanocomposites offer a new premise in the development of next-generation materials with novel properties and wide applications.

2.1.3 Nanocomposites

Nanocomposites constitute a special class of materials consisting of two or more phases, with at least one of the phases in the nanoscale range. Composite materials are not new in nature – various naturally occurring substances are some or the other form of composites only, e.g., bamboo, clay, milk, etc. are all composites of different types of materials. Similarly, the enamel of teeth and bones of higher vertebrates including humans are nothing but nanocomposites of hydroxyapatite and other protein molecules. These natural composite materials exhibit a unique blend of properties which are not present in the constituents themselves. For instance, even though tooth enamel is 95% hydroxyapatite, small amounts of proteins play a significant role in its observed toughness (Braun 2003). Likewise, the dragline spider silk which constitutes the spokes in a spider web, is five times tougher than steel by weight and can stretch 30-40% without breaking (Braun 2003). These and numerous other examples in biology are a direct verification of the advantages of nanocomposites over conventional materials. Taking inspiration from these natural composites, various research groups have been working on the development of novel nanocomposites for different applications.

Such engineered nanocomposite materials are fast replacing the conventional microcomposites and monolithics. These materials, due to very small (≤ 10 nm) grains and a significant role of boundary regions surrounding individual grains, exhibit enhanced or even completely new properties, and behave in a strongly different manner compared to the conventional materials composed of larger (≥ 100 nm) grains (Mukhopadhyay and Basu 2013; Musil 2012). For instance, the addition of CNT in alumina matrix increases its toughness and at the same time reduces its coefficient of friction considerably (Puchy et al. 2013). CNT addition has also been reported to improve the thermal properties of alumina (Kumari et al. 2008). Hybrid organic-inorganic nanocomposites have also been developed which exhibit improved mechanical and oxidation stability, decreased solvent uptake, recyclability and tuneable biodegradability (Sorrentino et al. 2007). Thus, there is sufficient evidence to claim that nanocomposites, indeed, have the potential of giving rise to a whole new class of high-performance materials.

Typically, a nanocomposite consists of a continuous “matrix” phase and one or more discontinuous “reinforcer” phase(s) embedded in the matrix. Although different types of nanocomposites have been synthesized using different combinations of matrix and reinforcers, they have been majorly divided into three types:

- Ceramic based nanocomposites
- Metal based nanocomposites
- Polymer based nanocomposites

Of these, ceramic based nanocomposites have gained huge attention owing to improved mechanical and electrical properties. Conjugating ceramics such as alumina, zirconia etc. with other materials decreases their brittleness along with a synergistic improvement in their electrical properties, thus improving their utility in various applications, such as electrochemical sensors, supercapacitors, Li-ion batteries, etc. (Jiang et al. 2012; Jiang et al. 2014; Wu et al. 2012). Among the diverse repertoire of ceramic nanocomposites, yttria-stabilized zirconia nanocomposites (YSZ) has emerged as one of most extensively researched composite materials, owing to their interesting properties. It has been reported that YSZ nanocomposites exhibit considerable superplasticity at relatively high strain rates (Mukhopadhyay and Basu 2013). In addition, they possess high structural stability and biocompatibility and low thermal conductivity, which has enabled the use of this composite in the development of thermal barrier coatings, solid oxide fuel cells and dental fillers (Tredici et al. 2016).

The advent of carbon-based nanomaterials has further led to the development of a new class of carbon/metal oxide nanocomposites. Carbon nanotubes (CNT) have been the most widely used carbon-based nanomaterial for the development of metal oxide-based nanocomposites. Reports have indicated that conjugation of CNT with metal oxides such as

Al_2O_3, MnO_2, ZnO, etc. leads to improved mechanical, tribological, thermal and electrochemical properties (Afsharmanesh et al. 2013; Puchy et al. 2013; Xia et al. 2012). However, the inherent difficulties in the synthesis of CNT combined with the high costs of processing have limited their applications. rGO is another carbon-based nanomaterial having a higher surface area and electrochemical activity than CNT (Shao et al., 2007). Unlike CNT, which are mostly used as filler in nanocomposites, rGO can be used as a matrix for the grafting of other nanomaterials.

2.1.3.1 Yttria-stabilized zirconia

Zirconium dioxide (ZrO_2), or zirconia as it is commonly called, is a white-colored oxide of group IV transition metal zirconium. Like other metallic nanoparticles, nanostructured ZrO_2 ($nZrO_2$) exhibits enhanced electrical conductivity and possesses high surface area. In addition, it exhibits high chemical inertness, biocompatibility, and relatively high mechanical, thermal and structural stability. The surface of $nZrO_2$ possesses hydroxyl groups rendering it easy to functionalize with a wide variety of chemical and biological moieties. Owing to these advantageous properties, $nZrO_2$ has found many applications in biomedical sciences. Mesoporous zirconia nanoparticles possessing high surface area have been synthesized for potential theranostic applications (Sponchia et al. 2015). Another study has reported the development of amine-functionalized lanthanide-doped zirconia nanoparticles-based luminescent bioprobes for targeted imaging of cancer cells (Liu et al. 2012). These bioprobes were also shown to detect avidin with a detection limit of 3 nM. Recently, an amine functionalized $nZrO_2$-based biosensing platform has been reported for non-invasive detection of CYFRA-21-1, an oral cancer biomarker, in human saliva (Kumar et al. 2016). This biosensing platform was shown to possess a remarkable detection limit of 0.1 ng mL^{-1} and a dynamic range that covers the whole physiological range of CYFRA-21-1. Thus, it is evident that $nZrO_2$ holds huge potential in a number of biomedical applications. However, single phase $nZrO_2$ possesses a few limitations which restrict its use for many applications.

Structurally, zirconia is polymorphic in nature, and exists in three phases – monoclinic, tetragonal and cubic depending upon temperature. Monoclinic zirconia is the most stable configuration at room temperature. Thus, tetragonal zirconia is shown to transform into monoclinic form with time which leads to a volume expansion of ~5%. Consequently, single phase zirconia crystals are brittle in nature (Lughi and Sergo 2010). This limits the use of pure single phase zirconia as a structural element for coatings, biomedical implants, sensors, etc. Reports have suggested that this transformation can be reduced and delayed for a long period by doping with other ceramics such as Y_2O_3, CeO_2, Al_2O_3, etc. (Fornabaio et al. 2015; Lughi and Sergo 2010). The most prominent among these binary systems is yttria stabilized zirconia (YSZ). To-date, only Y_2O_3-ZrO_2 system has attained an ISO status for surgical application (Lughi and Sergo 2010). Different mechanisms have been hypothesized to explain the stabilizing effect of Y_2O_3 on ZrO_2 structure. According to a theory, stress-induced tetragonal to monoclinic transition in YSZ crystals does not allow crack propagation in the crystal. This results in the high observed strength and toughness of YSZ crystals (Fornabaio et al. 2015; Palmero et al. 2014). Furthermore, it has been suggested that reducing the size of grains in YSZ crystals to nanoscale could result in improved stability of tetragonal phase of zirconia at room temperature (Lughi and Sergo 2010).

The addition of Y_2O_3 into ZrO_2 crystal lattice may lead to significantly higher electrical properties of the YSZ systems (Zhang et al. 2007). Reports have confirmed that due to the displacement of some of the Zr^{4+} ions by the relatively smaller Y^{3+} ions in the crystal lattice of zirconia, oxygen vacancies are generated in the lattice space. These oxygen vacancies are responsible for the high ionic conductivity displayed by YSZ ceramics at high temperatures (Jang et al. 2015; Scherrer et al. 2013). It has also been observed that the presence of oxygen vacancies may further enhance mechanical stability of the YSZ ceramics (Lughi and Sergo 2010). According to some other reports, much of the conductivity displayed by nancrystalline and porous YSZ films is due to the protons generated by the breakdown of adsorbed interfacial water molecules (Jang et al. 2015; Miyoshi et al. 2014; Scherrer et al. 2013).

These properties have enabled the use of YSZ films and crystals in a wide range of applications, such as thermal barrier coatings, solid oxide fuel cells (SOFC), dental fillers, biomedical implants, gas sensors, etc. (Chan et al. 2013; Le Coadou et al. 2015; Noh et al. 2014; Palmero et al. 2014; Tredici et al. 2016). Low temperature degradation resistant nanostructured YSZ has been developed with potential applications in periodontics (Tredici et al. 2016). Another study has reported the fabrication of thin films of YSZ having potential applications in ultrathin implantable devices (Le Coadou et al. 2015). It is worth noting here that most of the biomedical applications of YSZ take advantage of only the mechanical stability of YSZ ceramics. The electrochemical properties of nanostructured YSZ are limited only to the development of SOFCs and gas sensors only. Efforts are needed to further explore the potential of YSZ in other applications such as biosensing, wherein both the mechanical and electrochemical properties of YSZ could be of great advantage.

2.1.3.2 Reduced graphene oxide

Reduced graphene oxide (rGO) is a 2-dimensional sheet-like structure composed of sp^2-hybridized carbon arranged in a one-atom thick hexagonal honeycomb lattice (Gómez-Navarro et al. 2010). It is an analog of pristine graphene, with the only difference being the presence of a few oxygen-containing functional groups (Ali et al. 2016; Gómez-Navarro et al. 2010). The exceptional electronic properties have allowed the widespread use of this carbon allotrope in the development of electrochemical devices (Compton and Nguyen 2010; Song et al. 2016). Recently, it has also been employed in various biomedical applications, such as imaging, targeted therapy, and biosensing, owing to the presence of the functional groups that makes the immobilization of biomolecules easier (Kumar et al. 2016; Shao et al. 2010). The extent of research into the biomedical applications of rGO is highlighted by the vast amount of literature available on the subject (Bitounis et al. 2013; Chung et al. 2013; Shen et al. 2012). Recently, Reiner-Rozman et al. have reported efficient functionalization of rGO with a variety of biomolecules, such as antibodies, peptides, etc. and used it as gate material in FET sensors for the detection of various analytes including BSA, aflatoxin B1 and smell odorants (Reiner-Rozman et al. 2016).

rGO-based nanocomposites have emerged as a new class of composite materials which combine the exceptional electrical property of rGO with those of other (nano-)materials. Particularly, a spectacular evolution of graphene–transition metal oxide hybrid nanomaterials (nMOx-rGO) has been witnessed in electrochemical fields owing to the exceptional electrochemical and structural properties of GR as well as the catalytic characteristics of nMOx (Ali et al. 2016; Khan et al. 2015; Kumar et al. 2016; Shin et al. 2013). Another advantage displayed by rGO/nMOx hybrid nanocomposites is increased dispersibility of rGO in aqueous systems due to increase in the inter-atomic distance between individual sheets of rGO. This also prevents stacking of rGO nanosheets leading to improved electrocatalytical properties. Furthermore, the agglomeration of nMOx is also prevented due to grafting on rGO sheets. As a consequence, nMOx-rGO nanocomposites display synergistic improvement in their mechanical and electrochemical properties (Ali et al. 2016; Khan et al. 2015; Srivastava et al. 2015).

nMOx-rGO nanocomposites are finding a wide range of applications ranging from Li-ion batteries, supercapacitors and photocatalysis to biosensors, drug delivery, and adsorbent materials (Khan et al. 2015; Srivastava et al. 2015). Since it is beyond the scope of the present work to summarize all the reports on the vast number of applications of nMOx-rGO nanocomposites, biomedical applications have been briefly discussed with particular focus on biosensors. Recently, nMOx-rGO nanocomposites have emerged as the preferred choice for the development of electrochemical biosensors for clinical diagnostics. Ali et al. have reported the development of an rGO-NiO based biosensing platform for the detection of low-density lipoproteins (LDL) in a wide linear range of 0 – 130 mg/dL (Ali et al. 2016). Yang et al. demonstrated that nanocomposite of ZrO_2 with electrochemically reduced graphene oxide (ZrO_2-ERGNO) allows accessible space for DNA hybridization to occur and thus results in a remarkable detection limit of 1.21×10^{-14} M for DNA sensing (Yang et al. 2013). Jiang et al. have reported on the development of an ultrasensitive biosensor based on ZnO-graphene nanocomposite for detection of the pharmaceutically-relevant acetaminophen and phenacetin molecules (Jiang et al. 2014). This biosensor exhibited a sensitivity of 54 295.82 $\mu A\ mM^{-1}\ cm^{2}$ for acetaminophen and 21 344.66 $\mu A\ mM^{-1}\ cm^{2}$ for phenacetin, respectively. Recently, Kumar et al. have reported on the development of a ZrO_2-rGO based biosensing platform for the detection of an oral cancer biomarker in human saliva (Kumar et al. 2016). This biosensing platform exhibited a wide linear range and enhanced sensitivity. Other reports have also verified the importance of nMOx-rGO nanocomposites in the fabrication of biosensors, which are being seen as the future of health care and clinical diagnostics.

2.2 Biosensor

Since the landmark invention of a glucose sensing electrode by Leland Clarke in 1962, biosensors have become the subject of extensive research. According to the IUPAC, a biosensor is defined as “a self-contained integrated device that is capable of providing specific quantitative analytical information using a biological recognition element (biochemical receptor) which is in direct spatial contact with a transducer element.” In other words, biosensor is an analytical device which converts a biological signal into an observable electrical (or, electronic) signal via a transducer. A biosensor typically has five components: (i) bio-recognition molecules, (ii) immobilization matrix, (iii) transducer, (iv) amplifier, and (v) digital readout. Each of these components is essential for the structural and functional integrity of a biosensing device. The performance of a biosensor is evaluated on the basis of seven parameters. These parameters are – (i) sensitivity, (ii) selectivity, (iii) response time, (iv) shelf life, (v) stability or reusability, (vi) recovery time, and (vii) accuracy. An ideal biosensing device is one which has a high sensitivity, selectivity and accuracy with a low response time.

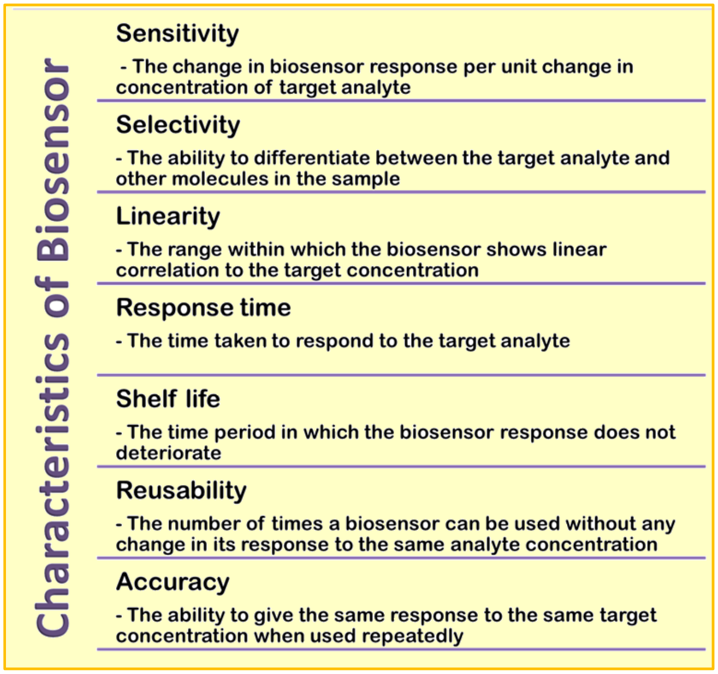

Characteristics of Biosensor

Sensitivity	- The change in biosensor response per unit change in concentration of target analyte
Selectivity	- The ability to differentiate between the target analyte and other molecules in the sample
Linearity	- The range within which the biosensor shows linear correlation to the target concentration
Response time	- The time taken to respond to the target analyte
Shelf life	- The time period in which the biosensor response does not deteriorate
Reusability	- The number of times a biosensor can be used without any change in its response to the same analyte concentration
Accuracy	- The ability to give the same response to the same target concentration when used repeatedly

Figure 2.2 Characteristics of a biosensor

With improvement in our understanding of electroanalytical techniques, biosensing technology has evolved over time and different generations of biosensors have emerged depending upon the intimacy between electrode and biomolecules and the presence or absence of certain mediators.

- First generation biosensors involved the separation of substrate and the reaction products from the transducer surface by a porous membrane. An electrical response was generated when the reaction products crossed the membrane to interact with the transducer.
- Second generation biosensors introduced the use of specific 'mediators' which acted as electron transporters between the immobilized biorecognition element and the transducer. Thus, an improvement in response was achieved.
- Third generation biosensors integrated the biological signal directly to the transducer surface using direct immobilization strategies.

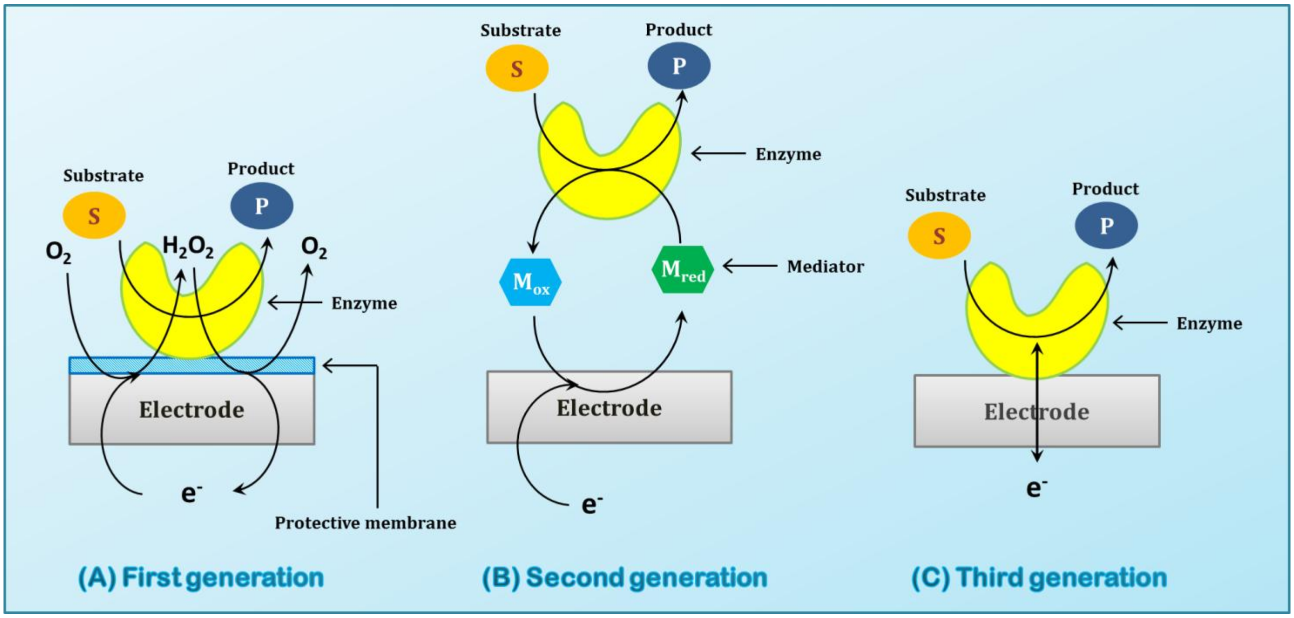

Figure 2.3 The three generations of biosensors

Biosensors possess many advantages over conventional detection assays, some of which are –

- Requirement of low sample volume
- High sensitivity and specificity
- Detection in the ultralow pM-fM range is possible
- Fast response
- Possibility of real-time analysis
- Continuous monitoring is possible
- Multiplexed detection is feasible
- Ability of being miniaturized
- Possibility of batch production
- Point-of-care (POC) applications are possible

2.2.1 Components of biosensor

As discussed above, a biosensor consists of three major components as shown in **Figure 2.3**. These are – (i) bio-recognition element (biomolecules, e.g., antibodies, etc.), (ii) immobilization matrix providing surface for immobilization of bio-recognition element, and (iii) a transducer for conversion of the biological signal to a recognizable signal which may be electrical, optical or physical in nature.

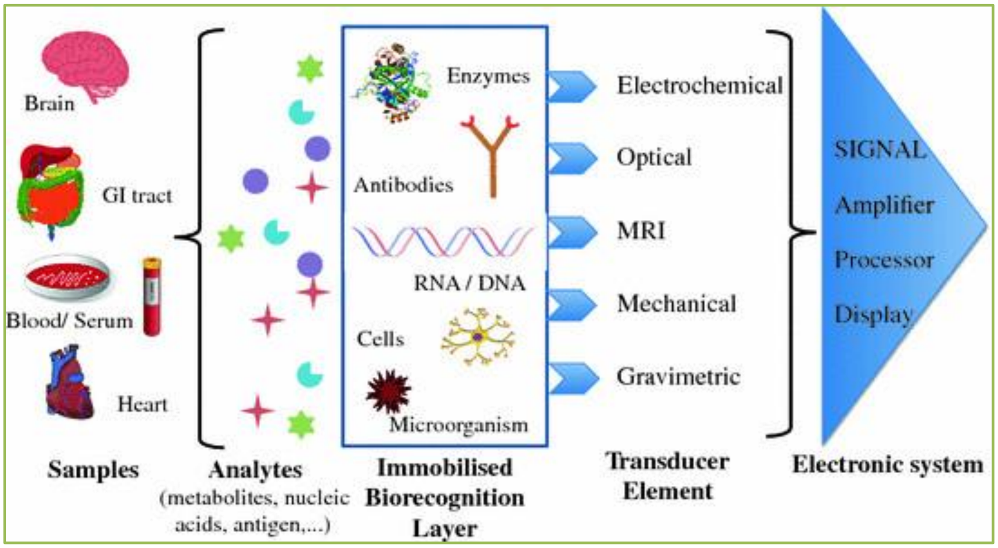

Figure 2.4 Components of a biosensor

2.2.1.1 Bio-recognition element

A bio-recognition element is a biomolecule or a molecular assembly possessing the ability to interact specifically with another substrate/analyte. On the basis of the type of biorecognition element utilized, biosensors have been classified into –

- Enzyme-based biosensors (catalytic biosensors) – these biosensors rely on the enzymatic conversion of the target analyte
- Antibody based biosensors (immunosensors)
- Aptamer or DNA-based biosensors (genosensors)
- Cell-based biosensors

The first biosensing device, the blood glucose analyzer, utilized GOx enzyme as a bio-recognition element for the detection of glucose in whole blood. Enzymes are still prominently used in the development of electrochemical (amperometric or potentiometric) biosensors. A primary advantage of using enzymes as bio-recognition elements is that the enzyme-substrate reactions are often associated with electron release/capture. This directly leads to the change in the current flowing across the transducer which can be easily amplified and recorded. It is worth noting here that the activity of enzymes is highly susceptible to changes in its 3D structure, pH and presence of impurities which might act as inhibiting agents. Thus, the immobilization of enzymes has to be carried out carefully and with precision such that the active sites of the enzyme remain available for reaction. With advances in analytical technologies, different types of transducers came into light enabling the use of other types of bio-recognition element. Antibodies, a class of immunoglobulins, have been the most popular choice for biosensor development for a long time now. They possess high affinity for their target (antigen) and have been in clinical use for sensitive detection of many disease-related biomarkers. Furthermore, they can be designed and synthesized *in vitro* as per the need. The use of antigen-antibody interactions in biosensors was first limited by the fact that they do not usually accompany a direct recognizable change in electrical flow across through the transducer. This problem has been resolved with the introduction of redox mediators in the biosensing platform. The direct integration of antibody-antigen interactions with the transducer surface could lead to a change in the interfacial kinetics of the transducing surface which can be detected by various techniques. Ultrasensitive transducers detecting change in mass of a few µg at their surface (piezoelectric) have also been utilized for detecting antigen-antibody interactions. Now-a-days, affibodies, a class of affinity peptides, have also emerged as potential bio-recognition elements for biosensors. These peptides possess high affinity for their target which is comparable to those of antibodies, and in turn are less bulky and easily immobilizable in comparison to immunoglobulins. Recently, aptamers, short-chain oligonucleotides, and DNA have also been utilized for sensitive detection of a number of DNA species in body fluids. Such biosensors rely on DNA hybridization reactions and often use electrochemical transducers for detection of the same. These biosensors have found applications in clinical diagnostics and have been utilized for the detection of various disease related biomarkers present in body fluids. Whole cell biosensors utilizing microbial cells as bio-recognition elements are also being developed for potential use in environmental monitoring. Yeast cells have been utilized for the fabrication of a biosensor for fast measurement of biological oxygen demand (BOD). Similarly, bacterial cells have also been immobilized onto biosensing platforms for the detection of pollutants and heavy metals in waste water. Such biosensors rely on the conversion of target analyte via enzymes present in the whole cells. This has the advantage that the enzymes remain in their native physiological state and retain their activity for long periods. However, biofouling is a major concern for whole cell biosensors.

2.2.1.2 Immobilization matrix

The material composition of the biosensing surface on to which the biological sensing element is immobilized is of prime importance. Earlier, immobilization matrixes were utilized solely to provide a native environment to the biomolecules for their proper activity and function. As biosensors evolved, such matrices became more directly involved in enhancing the capability of transducers. Thus, immobilization matrices are essential for both the structural and functional integrity of biosensors. An ideal matrix should be such that it does not interfere with the functional activity of biomolecules and at the same time enables intimate contact with the transducer surface. In addition, such as surface should also possess non-interference to detection of target analyte, high surface area for immobilization, biocompatibility, non-toxicity, chemical inertness and structural stability. In this context, nanomaterials have emerged as efficient immobilization matrices for biosensors owing to their unique mechanical, optical, thermal and electrical properties. They provide a large surface area enabling high loading of biomolecules. In addition, they can be easily functionalized via a number of different conjugation chemistries due to their surface reactivity. In addition, it has been reported that nanomaterial-based biosensors possess enhanced signal amplification, higher signal transduction rate and better performance in terms of sensitivity and selectivity (Malhotra et al. 2016; Wang 2005; Zhu et al. 2014). Furthermore, the ability to tailor the size and electrocatalytical properties of nanomaterials allows for the development of novel biosensing interfaces which are sensitive down to the single molecule level (Besteman et al. 2003; Crespilho et al. 2009; Holzinger et al. 2014). These benefits have aroused scientific interest into the development of nanomaterial-based biosensors.

nMOx-rGO as immobilization matrix

nMOx-rGO nanocomposites have gained recent attention as biosensing platforms owing to the combined properties of rGO and nMOx. rGO has a high electron transfer rate along with a high surface area, while nMOx offer ease of functionalization, high electrical conductivity and improved structural stability. Out of the diverse nMOx available, composites of $nZrO_2$ with rGO have shown great potential in sensing applications. The properties of rGO and $nZrO_2$ have been discussed in earlier Sections. In brief, $nZrO_2$-rGO nanocomposites display a synergistic improvement in their electrochemical and mechanical properties and a net reduction in the agglomeration of $nZrO_2$ (Kumar et al. 2016; Teymourian et al. 2014). In addition, these composites are biocompatible and can be readily obtained in thin films. These properties make $nZrO_2$-rGO an ideal candidate for biosensing platforms. A recent study has reported on the development of $nZrO_2$-rGO based biosensor for simultaneous detection of uric acid, ascorbic acid and urea via electrochemical technique (Teymourian et al. 2014). Another study has reported that nanostructured composite of ZrO_2 with electrochemically reduced graphene oxide (ZrO_2-ERGNO) allows accessible space for DNA hybridization to occur and thus results in a remarkable detection limit of 1.21×10^{-14} M for DNA sensing (Yang et al. 2013). Recently, a ZrO_2-rGO based biosensing platform has been developed for detection of oral cancer biomarker in saliva (Kumar et al. 2016).

2.2.1.3 Transducer

In the context of biosensors, a transducer is a device which converts biological signal to a recognizable signal which may be electrochemical, optical or piezoelectric in nature. On the basis of the transducing mechanism, there are majorly three different types of biosensors: (i) electrochemical, (ii) piezoelectric and (iii) optical. Out of these, electrochemical biosensors have gained much attention owing to their ease of fabrication and fast response time. According to Kang *et al*., electrochemical biosensors are actually "bioelectronic interfaces" which combine the affinity and specificity of biomolecular recognition molecules with an electrochemical interface (e.g., an electrode) leading to fast and reliable results (Kang et al. 2012). They possess high signal-to-noise ratio, possibility of batch production, lower costs, low power requirements, high sensitivity and fast response times (Wang 2005). Electrochemical biosensors have been successfully employed in a number of different applications, such as monitoring of blood glucose levels, detection of pathogens, environmental monitoring, cancer diagnosis, etc. (Chikkaveeraiah et al. 2012; Singh et al. 2013; Wang 2008; Zhang et al. 2014).

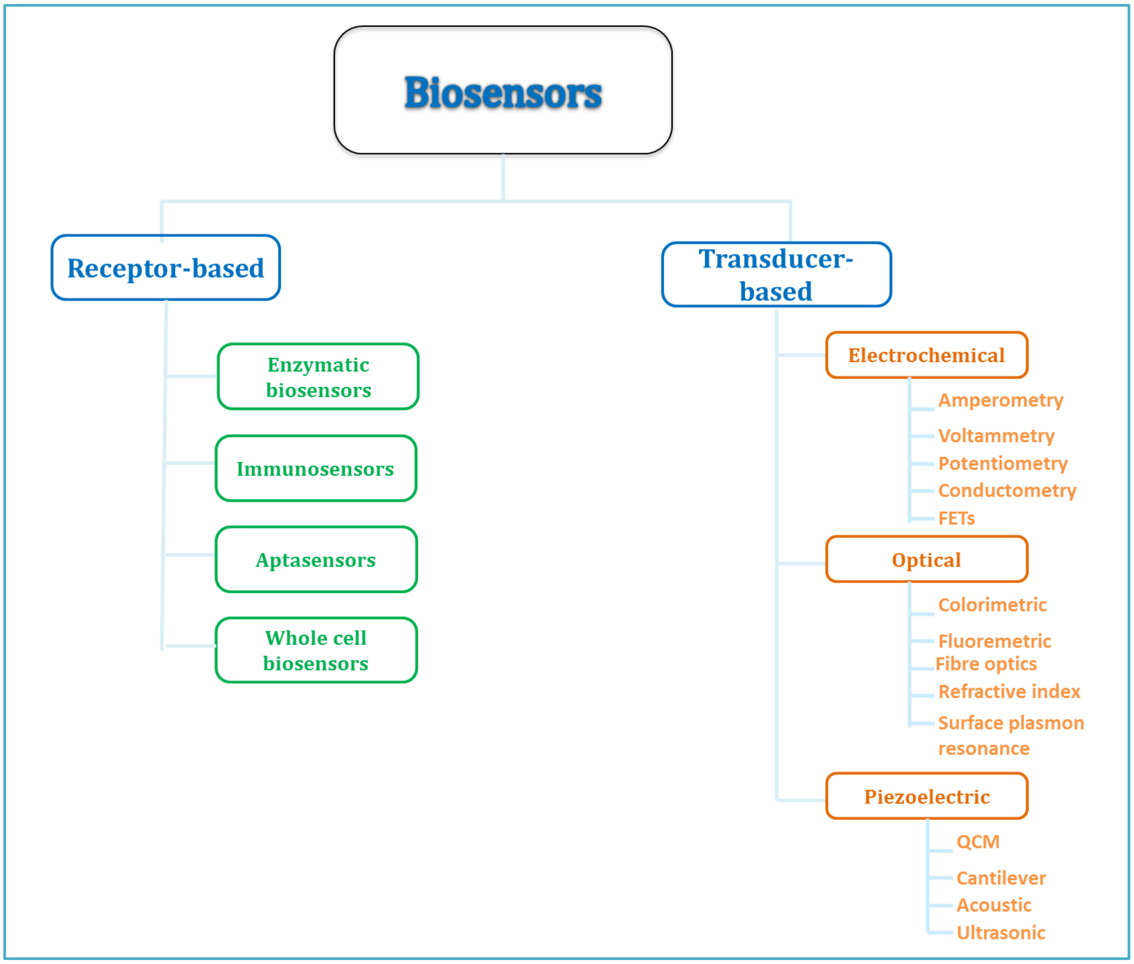

Figure 2.5 Different types of biosensor

2.2.2 Applications of biosensors

Since their introduction, biosensors have found diverse applications in different fields including, homeland defense, food safety control, bioprocess monitoring, environmental monitoring, pathogen detection, molecular diagnostics, etc. (Mishra et al. 2016; Nikoleli et al. 2016; Singh et al. 2013; Zhang et al. 2014). The first device referred to as a biosensor was the blood glucose analyzer which was based upon Clark's oxygen sensing electrode technology. This device measured the difference in the pO_2 levels when glucose oxidase (GOx), entrapped on the electrode via a semipermeable membrane, converted relatively electroinactive glucose into electroactive hydrogen peroxide. Since then, different biosensing technologies have been utilized to detect glucose and other clinically important analytes and metabolites, such as urea, lactate, dissolved gases, etc. However, one of the most important applications of biosensor has been cancer detection and monitoring. Significant amount of research has been devoted to the development of POC biosensors which can be utilized outside a central facility for detection of different types of cancer-related markers in biological fluids. Such devices can also be utilized for continuous monitoring of cancer which is at present a time-consuming and expensive procedure. Thus, biosensors could prove to be a cost-effective solution to the detection and monitoring of cancer.

Many biosensors have been reported for cancer diagnosis and screening in the recent past, which detect specific cancer-related antigens, miRNA species or DNA mutations (also called "biomarkers") whose concentration in body fluids, such as serum, urine, etc. are correlated to the presence of cancerous tumor or malignancy (Feng et al. 2011; Jin et al. 2014; Laschi et al. 2014; Ren et al. 2013). A recent study has reported the development a DNA-graphene-polypyrrole based nanobiosensor for the detection of DNA mismatch repair proteins at nanomolar levels for colorectal cancer diagnostics (Macwan et al. 2016). A GO-based aptameric paper nanbiosensor has also been reported which utilizes microfluidics for the multiplexed detection of cancer cells (Liang et al. 2016). In a novel approach, a study has reported the development of an antibody-free microwave biosensor for the detection of cancer cells in culture (Wu 2016). This biosensor was used to detect various cancer cells such as HepG2, A549 and HEC-1-A via the changes in their dielectric properties. A highly sensitive electrochemical biosensor has been reported for the detection of miRNA155, a breast cancer biomarker, in attomolar level (Cardoso et al. 2016). This biosensor exhibited a detection limit of 5.7 aM in human serum samples. Thus, it is clear that biosensors can prove efficient tools for the detection and monitoring of cancer.

2.3 Cancer

From a cytological point of view, every living organism is made up of a number of different cells performing specific functions in an integrated manner. Almost all of these various types of cells in the body have a finite life span after which stop performing their normal functions and undergo apoptosis – a natural cell death process. The dead cells are replaced with newly proliferated cells, thus a fine balance is maintained between the cell death and cell renewal such that the number of cells in a living organism remains fairly constant over its lifetime. However, in certain instances, a few “transformed” cells fail to respond to normal growth regulatory mechanisms and start proliferating indefinitely in an uncontrolled manner. Such “immortal cells” divide rapidly into more number of abnormal clones and give rise to a condition referred to as cancer and the cells are referred to as cancerous cells. In other words, cancer is defined as rapid, uncontrolled growth of cells due to the presence of multiple aberrations in the cellular genome.

According to the WHO, 14 million cases of cancer have been reported so far worldwide (Ferlay et al. 2015). It is currently the second most death-causing disease in the world topped preceded only by cardiovascular diseases. Among the various types of cancers, lung cancer is the most common death-causing cancer, followed by breast and gastrointestinal cancer. With changes in lifestyles and increase in environmental pollutions, the situation could get grimmer. The burden of most of these cancers is higher in the more developed regions of the world due to sedentary lifestyles, increased reliance on processed foods, higher exposure to carcinogens and increased genetic susceptibility. However, the burden of cancer in the developing and less developed regions of the world is estimated to increase and may even surpass those in the developed ones.

2.3.1 Oral Cancer

Oral cancer has become a major problem worldwide and is currently the 6th most common death-causing cancer in the world. According to the WHO, around 300, 000 cases of oral cancer (lip and oral cavity) were known in 2012 worldwide, with two-thirds of them being men (Ferlay et al. 2015). The situation is even more grim in Asia which is indicated to be the home of around half of the world’s total oral cancer cases (including at-risk subjects) as of 2012. It is the third most common cancer in India after cancers of the breast and cervix (Rajaraman et al. 2015). Moreover, India is presently the oral cancer hub in the world, with the highest number of incidence and mortality cases (**Figure 2.6**). The present scenario highlights the need for awareness towards oral cancer and development of cost-effective diagnostic technologies. Over 90% of malignancies affecting the oral cavity and maxillofacial region, are squamous cell carcinomas (OSCC) (Das and Nagpal 2002; Johnson et al. 2011). OSCC is usually preceded by precancerous lesions, such as leukoplakia, erythroplakia and oral submucous fibrosis (OSMF), which are morphologically altered tissue with a high risk of getting cancerous (Das and Nagpal 2002).

A number of reasons could be accounted for malignant transformation in the oral epithelia. The major risk factors for oral cancer, especially in countries like India, include poor oral hygiene, tobacco and betel quid chewing, smoking, poor nutrition, human papillomavirus (HPV) infection and a general lack of awareness among the masses (Johnson et al. 2011; Kumar et al. 2015; Zygogianni et al. 2011).

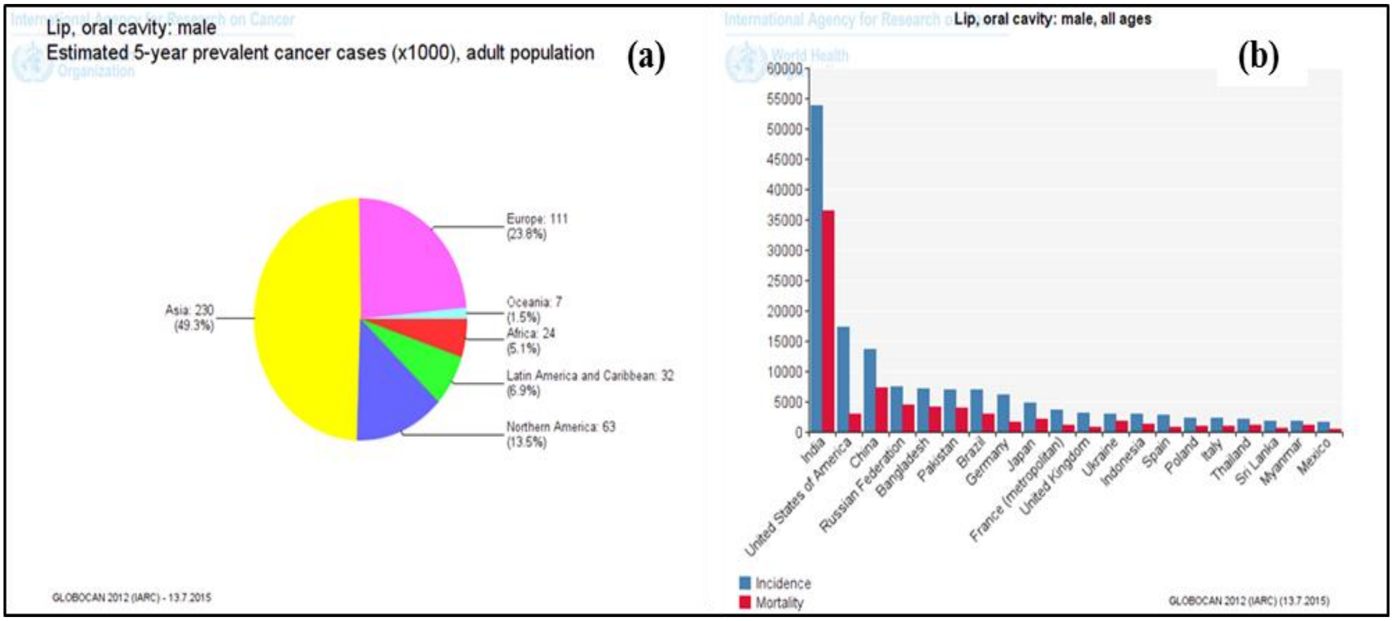

Figure 2.6 (a) 5-year prevalence of oral cancer in male adult population in major regions of the world, **(b)** top 20 nations in the world in terms of incidence and mortality (in numbers) of oral cancer

2.3.1.1 Conventional techniques for oral cancer detection

Conventionally, biopsy is the most prominent technique used for the diagnosis of oral cancer. However, since biopsy requires surgical procedure, it is usually preceded by other tests which can detect the presence of malignant transformation, such as toluidine blue dye test, cytological brush tests, light-based systems, etc. (Mehrotra and Gupta 2011; Rajaraman et al.

2015). These techniques are also used as adjunct aids in the diagnosis of oral cancer. These techniques have been summarized below –

(i) **Surgical biopsy** – It is currently the center of oral cancer diagnosis regime. It consists of taking out a sample of tissue from the affected area and analyzing it histopathologically for cancer-related transformations. There are three types of biopsy available depending on the region affected – punch biopsy, fine needle aspiration (FNA) and panendoscopy.

(ii) **Toluidine blue dye test –** It is based on the principle that tolonium chloride, a metachromatic dye, selectively stains cancerous cells blue. On the other hand, healthy cells do not take up this dye.

(iii) **Light-based systems –** The principle behind these systems is that cancerous cells have different absorbance and reflectance properties from healthy cells, e.g., abnormal cells reflect light and appear brighter, whereas healthy cells appear blue in 490-510 nm wavelength of light (Rajaraman et al. 2015).

(iv) **Brush cytological tests –** In this procedure, a specialized brush is used to obtain a transepithelial biopsy specimen which is then studied under the microscope for cancerous cells. It is being seen as a painless alternative to incisional biopsy.

Though these tests are of appreciably high diagnostic value, they possess a number of limitations. Surgical biopsy requires the application of local anesthesia and can be particularly uncomfortable and may even cause bruises. Other limitations of biopsy include invasiveness, artefacts in oral tissue samples leading to misinterpretation, inter-observer variability in histological diagnosis, etc. (Mehrotra and Gupta 2011). The other tests are associated with high variations in sensitivity, and the test results are often based on subjective interpretation (Awan et al. 2011; Lingen et al. 2008; Rajaraman et al. 2015). In addition, several studies have reported the lack of consistent evidence to prove the efficacy of these adjunct aids (Giovannacci et al. 2016; Lingen et al. 2008; Patton et al. 2008). It is also worth noting that all these techniques require the presence of trained professionals and cannot be used for continuous assessment due to high costs. Biopsy particularly, is laborious and time consuming. Thus, there is a huge need for a sensitive diagnostic tool which gives results in lesser time and can be used for continuous assessment as well.

The advancements in analytical approaches have fuelled research into the development of other techniques which are less invasive than biopsy while giving reliable results. Efforts are being made to enhance the sensitivity of the optical aids already in use for oral cancer detection. Antibody-tagged photosensitizers and gold nanoparticles have been used for differential labeling of cancerous tissues in the oral cavity (El-Sayed et al. 2005; Low et al. 2016). Fluorescence spectroscopy and FT-IR have also been utilized for the detection of oral cancer (Kanniyappan et al. 2016; Menzies et al. 2014). However, the most promising novel approach towards oral cancer detection has been offered by the field of proteomics and metabolomics. The emergence of these analytical approaches has led to the development of advanced tools which enable the molecular profiling of different tissues in a matter of a few hours. This has facilitated the demarcation of differences between cancerous and health tissues at the most basic molecular level. In other words, proteomics has enabled the discovery of a number of molecules whose expression in cancerous microenvironment is drastically different from that in the healthy one (). These clinically significant molecules have been referred to as “biomarkers.” Different proteins, RNA and DNA species involved in the regulation of cell cycle, cell proliferation and tumor suppression have emerged as novel biomarkers for oral cancer.

2.3.1.2 Biomarkers

According to the US National Institutes of Health's (NIH), "a biomarker is a characteristic that is objectively measured as an indicator of normal biological processes, pathogenic processes, or a pharmacological response to a therapeutic intervention."In other words, biomarkers are those biological species whose concentrations are strongly correlated to the presence of a disease. Since cancer results from mutations in the cellular genome, it is associated with changes in the molecular extra- and intra-cellular microenvironment. Currently, a large number of protein, DNA and RNA species are known as cancer biomarkers. Some of them are even being used in clinical analysis of cancer, such as CEA, BRCA1, CA15.3, etc. The same is true for oral cancer. Molecular profiling of cancerous cells has revealed numerous differences in the microenvironment of cancer and healthy cells in the oral cavity. Many of these biomolecules have been pre-validated as oral cancer biomarkers. Moreover, the concentrations of several biomolecules in the body fluids, including serum, saliva, urine, etc. have been found to be drastically altered in oral cancer, including IL-1, IL-6, IL-8, endothelin-1, TNF, ORAOV DNA species, miRNA, etc.

Though biomarkers are present in all body fluids, saliva has emerged as a natural choice for diagnosis of oral cancer. Due to the diffusive properties of saliva, it has been referred to as "the mirror of the human body (Mishra et al. 2016)." It offers several advantages as a diagnostic medium over other bodily fluids, such as straightforward sample collection, non-invasiveness, easy access, sufficient quantities for analysis, easy processability, low costs for storage and transportation (Katakura et al., 2013; Liu et al., 2012). Several studies have confirmed that the levels of certain proteins, DNA species and miRNA are elevated in the saliva of oral cancer patients (Brailo et al. 2012; Elashoff et al. 2012; Mishra et al. 2016; Wei et al. 2011). Moreover, it is worth noting that the concentration of many of these markers is higher in saliva than in the serum obtained from the same patient, making it easier to detect biomarkers in saliva as compared to other body fluids, such as serum, or urine (Brailo et al. 2012). A comprehensive description of different salivary biomarkers for oral cancer has been provided in literature, including tumor suppressor genes (p53, CK16), growth factors (EGF, VEGF, IGF), cytokeratins (CK13, CK16, etc.), miRNAs, epithelial tumor factors (CYFRA-21-1), etc. (Bano et al. 2015; Mishra et al. 2016).

CYFRA-21-1 is one of the potential salivary biomarkers for oral cancer. It is released into the extracellular environment due to action of proteinases on cytokeratin-19, an intermediate filament (Bano et al. 2015; Cheng et al. 2014). It has been shown that there is a significant increase in the levels of CYFRA-21-1 in patients with OSCC as compared to healthy individuals. In addition, the levels of salivary CYFRA-21-1 have been reported to be 3 times higher than serum CYFRA-21-1 levels in oral cancer patients (Rajkumar et al. 2015). In a recent study, 312 blood samples from patients of head and neck cancers (HNC) were evaluated to determine the diagnostic and prognostic value of CYFRA-21-1 and three other tumour markers (Barak et al. 2015). The study observed that CYFRA-21-1 could serve as a diagnostic tumor marker for HNC and is prognostic for recurrence. The median CYFRA-21-1 concentration in normal human saliva has been reported to be 3.4 ng mL^{-1} while it can increase up to 13.2 ng mL^{-1} (median value) in oral cancer patients (Nagler et al. 2006). In addition, the levels of salivary CYFRA-21-1 has been reported in the range of ng mL^{-1} which is higher than those of other reported salivary markers (in the range of pg mL^{-1}) (Brailo et al., 2012; Rajkumar et al., 2013; Nagler et al., 2006), thus simplifying its detection to some extent (Brailo et al. 2012; Nagler et al. 2006; Rajkumar et al. 2015).

Biomarker source	Biomarker	Nature	Disease stage	Reference
Serum	C-reactive protein(CRP)	Protein	Diagnostic/Prognostic	(Jablonska et al. 1997)
	IL-1β	Protein	Diagnostic	Jablonska et al. 1997
	IL-6	Protein	Diagnostic	Mishra et al. 2016
	IL-8	Protein	Diagnostic	Mishra et al. 2016
	TNF-α	Protein	Diagnostic	Jablonska et al. 1997
	miRNA-184	RNA	Prognostic	Wong et al. 2008
	miRNA-31	RNA	Prognostic	Liu et al. 2010
	p53 antibodies	Protein	Diagnostic/Prognostic	Sainger et al. 2006
	Squamous cell carcinoma antigen (SCC-Ag)	Protein	Prognostic	Krimmel et al. 1998
	Sialic acid	Monosaccharide	Diagnostic	Mishra et al. 2016
	Endothelin-1 (ET-1)	Protein	Diagnostic	Mishra et al. 2016
	Fucose	Carbohydrate		Mishra et al. 2016
	CYFRA-21-1	Protein	Diagnostic/prognostic	Rajkumar et al. 2015
Urine	6-hydroxynicotic acid	Nicotine derivative	Diagnostic	(Xie et al. 2012)

	Valine	Amino acid	Diagnostic	(Xie et al. 2012)
	Tyrosine	Amino acid	Diagnostic	(Xie et al. 2012)
	Hippurate	Carboxylic acid	Diagnostic	(Xie et al. 2012)
	N-nitrosonornicotine (NNN)	Nitrosamine	Diagnostic	(Khariwala et al. 2013)
	1-hydroxypyrene (1-HOP)	Derivative of polyaromatic hydrocarbons (PAH)	Diagnostic	Khariwala et al. 2013
	Total NNAL	Nitrosamine	Diagnostic	(Boffetta et al. 2008)
	Cotinine	Alkaloid	Diagnostic	(Binnie et al. 2004)
Saliva	IL-1β	Protein	Diagnostic	Mishra et al. 2016
	IL-6	Protein	Diagnostic	Mishra et al. 2016
	IL-8	Protein	Diagnostic	Mishra et al. 2016
	MMP-9	Protein	Prognostic	(Shpitzer et al. 2009)
	Ki67	Protein	Prognostic	Schiptzer et al. 2009
	Mac-2 binding protein (M2BP)	Protein	Diagnostic	Elashoff et al. 2012
	Transferrin	Protein	Diagnostic	(Jessie et al. 2013)

	CYFRA-21-1	Peptide	Diagnostic/Prognostic	Nagler et al. 2006
	miRNA-125a	RNA	Diagnostic	Park et al. 2009
	miRNA-127	RNA	Prognostic	(Wiklund et al. 2011)
	miRNA-9	RNA	Diagnostic	Salazar et al. 2015
	Carnitine	Amino acid derivative	Diagnostic	Wang et al. 2014
	Choline	Vitamin	Diagnostic	Wang et al. 2014
	Phytosphingosine	Lipid	Diagnotic	Wang et al. 2014
	Succinic acid	Carboxylic acid	Diagnostic	Wang et al. 2014
	Cotinine	Alkaloid	Diagnostic	Binnie et al. 2004

Table 2.1 List of oral cancer biomarkers in serum, urine and saliva.

2.3.1.3 Biosensors for oral cancer detection

The development of quantitative techniques for salivary diagnostics has been rather slow due to limitations in sensitivity and detection ranges. Biosensors have emerged as an attractive option in this context. Serious efforts are being made towards the development of biosensor for oral cancer detection. A recent study presented an electrochemical DNA biosensor which could detect oral cancer-related DNA species present in saliva, at concentrations as low as 0.35 pM (Tan et al., 2015). Likewise, an ultra-highly sensitive electrochemical RNA biosensor has been reported which could detect oral cancer-related miRNA species at concentrations as low as 2.2×10^{-19} M (0.22 aM) in saliva (Wang et al., 2013). Another highlight of this biosensor is that it is electrically magnet-controllable which contributes to its ultra-high sensitivity.

Recently, Kumar et al. reported the development of nanostructured hafnia-based immunosensor for the detection of CYFRA-21-1 in human saliva (Kumar et al., 2016b). This study reported a wide linear range of 2-18 ng mL^{-1} with a detection limit of 0.2 ng mL^{-1}. On similar lines, two other studies have reported the development of $nZrO_2$ and $nZrO_2$-rGO based biosensing platform for non-invasive detection of oral cancer (Kumar et al., 2016a; 2015). Thus, it is clear that biosensors can be efficiently utilized for sensitive detection of cancer biomarkers.

In the present study, we have fabricated a novel biosensing platform based on nY_2O_3-$nZrO_2$-rGO nanocomposite and evaluated its performance against oral cancer biomarker CYFRA-21-1. Briefly, the nY_2O_3-$nZrO_2$-rGO nanocomposite was synthesized hydrothermally and subsequently functionalized via APTES. Thin films of the functionalized APTES/nY_2O_3-$nZrO_2$-rGO nanocomposite were obtained onto ITO electrodes via electrophoretic deposition. Anti-CYFRA-21-1 antibodies were subsequently functionalized onto this APTES/nY_2O_3-$nZrO_2$-rGO/ITO electrode followed by blocking of the non-specific sites by BSA. Differential pulse voltammetric studies were conducted to evaluate the response of the fabricated BSA/anti-CYFRA-21-1/APTES/nY_2O_3-nZrO_2-rGO/ITO immunoelectrode towards different concentrations of CYFRA-21-1.

Chapter 3

Materials and Methods

3. Materials and Methods

3.1 Materials

Yttrium nitrate hexahydrate [$Y(NO3)_3.6H_2O$] and zirconium ethoxide [$C_8H_2O_4Zr$] have been purchased from Alpha Aesar and Sigma Aldrich, respectively. Sodium hydroxide [NaOH] and N-cetyl-N,N,N-trimethyl ammonium bromide (CTAB) were obtained from SRL Chem and CDH, respectively. Sodium monophosphate [NaH_2PO_4], sodium diphosphatedihydrate [$Na_2HPO_4.2H_2O$], sodium chloride [NaCl], potassium ferricyanide {$K_3[Fe(CN)_6]$}, and potassium ferrocyanide {$K_4[Fe(CN)_6].3H_2O$} were purchased from Fisher Scientific. All chemicals were of analytical grade and were used without any further purification. The CYFRA-21-1 antigen biomarker and monoclonal anti-CYFRA-21-1 antibodies were procured frosm Ray Biotech, Inc., India. 0.05 mol each of $Na_2HPO_4.2H_2O$ and NaH_2PO_4, and NaCl (0.9%) were added to 1 L autoclaved MilliQ water to prepare fresh phosphate buffered saline (PBS) of pH 7. This PBS buffer was used to dilute the biomolecules to desired concentration and stored at -20 ˚C until further use. All electrochemical studies were carried out at room temperature.

3.2 Instrumentation

The following instruments and techniques have been utilized to conduct experiments reported in this work:

3.2.1 X-ray diffraction (XRD)

XRD studies were conducted on a Bruker D-8 Advance diffractometer. A monochromatic X-ray beam with Cu-Kα radiation (λ = 1.5406 Å) has been used to record the spectrum. XRD is based on constructive interference of monochromatic X-rays and a crystalline sample. These X-rays are generated by a cathode ray tube, filtered to produce monochromatic radiation, collimated to concentrate, and directed toward the sample. The interaction of the incident rays with the sample produces constructive interference (and a diffracted ray) when conditions satisfy Bragg's Law (**Eq. 3.1**)

$$2d \sin \theta = n \lambda \qquad \textbf{Eq. 3.1}$$

where, λ is the wavelength of electromagnetic radiation, θ is the diffraction angle and d is the lattice spacing in a crystalline sample. These diffracted X-rays are then detected, processed and counted. By scanning the sample through a range of 2θ angles, all possible diffraction directions of the lattice is attained due to the random orientation of the powdered material. This technique is used to characterize the crystallographic structure, crystallite size (grain size) and preferred orientation in polycrystalline or powder solid samples.

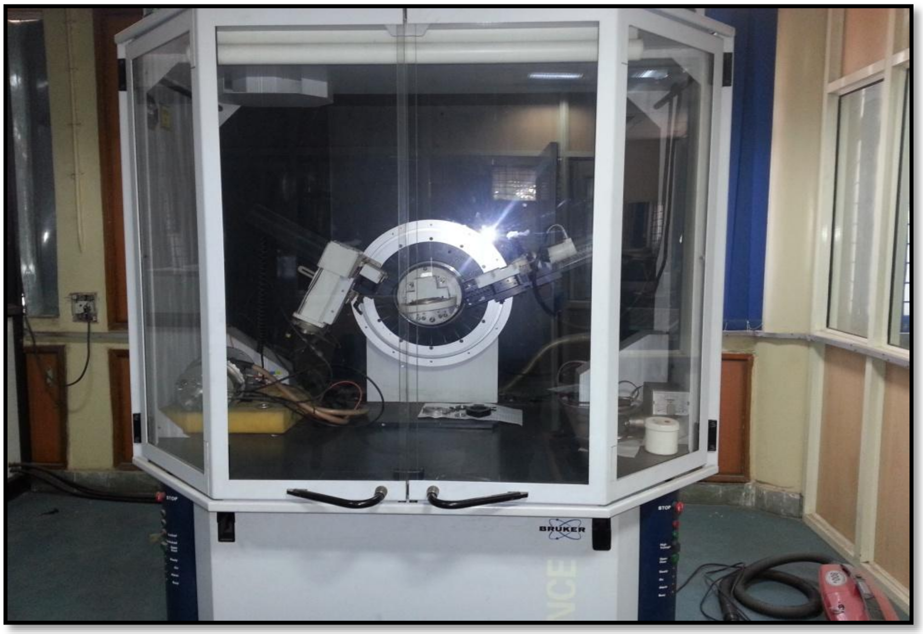

Figure 3.1 X-ray diffractometer (Bruker N8 Advance)

The mean size of the nanoparticles can also be determined from the peak broadening in the X-ray diffraction pattern by using Debye– Scherrer equation **(Eq. 3.2):**

$$D = \frac{0.9\lambda}{\beta Cos\theta} \qquad \textbf{Eq. 3.2}$$

where, D is the average crystallite size (Å), λ is wavelength of X-rays (Cu Kα: λ = 1.5418 Å), θ is the Bragg diffraction angle, and β is the full width at half maximum (FWHM) (in radians).

3.2.2 Scanning electron microscopy (SEM)

SEM analysis has been conducted to determine the morphology of the synthesized nanocomposite and the fabricated electrodes (Hitachi S-3700N). SEM is a powerful technique which utilizes a beam of highly energetic electrons to examine objects on a very fine scale. The electron beam is generated by a high energy source, e.g., heated tungsten, and scanned over a specimen. As the beam hits the specimen, electrons and X-rays are ejected from the sample which are collected by detectors and processed to produce a visual image of the fine structure of the sample. The resolution of SEM is around 10 nm allowing the visualization of materials at sub-micron levels.

Figure 3.2 Scanning electron microscope (SEM; S-3700N)

3.2.3 Fourier transform infrared (FT-IR) spectroscopy

FT-IR spectroscopy of the fabricated electrodes was conducted on a Perkin-Elmer instrument. FT-IR is an analytical technique used for the structural characterization of organic materials. It is based on the specific infra-red absorption displayed by molecular bonds depending upon their vibrational states. In the FT-IR spectra, the appearance or non-appearance of certain vibrational frequencies gives valuable information about the structure of a particular molecule. Each functional group has specific range of vibrational frequencies and is very sensitive to the chemical environment, thus providing valuable information regarding the presence of certain functional groups in the specific sample for their further characterization. FTIR spectrophotometer has a spectrum in the range of 400-4000 cm^{-1}.

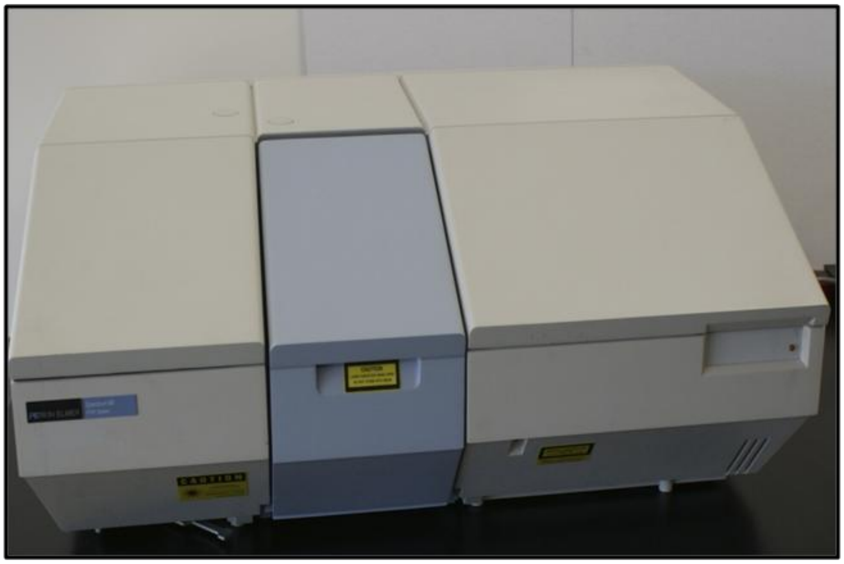

Figure 3.3 FT-IR spectrophotometer

3.2.4 Electrochemical studies

All electrochemical studies were conducted on an Autolab Potentiostat/Galvanostat (Metrohm, The Netherlands).These studies were conducted using a three-electrode system with ITO coated glass electrode as the working electrode, platinum (Pt) as the counter electrode, and silver-silver chloride (Ag/AgCl) as the reference electrode. PBS solution (50×10^{-3} M; pH 7) containing 5×10^{-3} M $[Fe (CN)_6]^{3-/4-}$ as redox species was used as the electrolyte.

Figure 3.4 Autolab Galvanostat/Potentiostat (Metrohm, The Netherlands)

Electrochemical techniques relate the changes of an electrical signal to an electrochemical reaction at an electrode surface, usually as a result of an imposed potential or current. In a solution, the equilibrium concentrations of the reduced and oxidized forms of a redox couple are linked to the potential (E) via the *Nernst's Equation* **(Eq. 3.3)**:

$$\mathbf{E = E_o + \frac{RT}{nF} \ln \frac{Coxi}{Cred}} \tag{Eq. 3.3}$$

where, Eo is equilibrium potential, F is Faraday's constant, T is absolute temperature, C_{oxi} and C_{red} are concentrations of oxidation and reduction centers. If the potential E is applied to the working electrode with respect to the reference electrode e.g. via Potentiostat, the redox couples present at the electrode respond to this change and adjust their concentration ratios according to **Eq. 3.3**.

3.2.4.1 Cyclic Voltammetry (CV)

Cyclic voltammetry is one of the most prominently used electroanalytical techniques for study of electroactive species and their properties. It involves the use of a triangular waveform for linear scanning of the potential of a stationary working electrode in an unstirred electrolyte. The resultant current is measured during the scan by a potentiostat and is plotted against the applied potential. This plot of current vs. potential is referred to as a cyclic voltammogram.

For a completely reversible system, the peak current is given by the Randles-Sevcik's equation –

$$\mathbf{I_p = (2.69 \times 10^5)\ n^{3/2}ACD^{1/2}\ v^{1/2}} \qquad \textbf{Eq. 3.4}$$

Where, I_p is the peak (cathodic or anodic) current, n is the number of electrons involved (1 for $[Fe(CN)_6]^{3-/4-}$), A is the area of the electrode surface in cm^2, C is the concentration of the redox probe in M, D is the diffusion coefficient and v is the scan rate in V s^{-1}. CV can be utilized for analysis of reaction mechanisms, redox potentials of unknown compounds and determination of concentrations of analytes.

3.2.4.2 Differential Pulse Voltammetry (DPV)

DPV consists of a series of potential pulses of fixed amplitude (10-100 mV) superimposed on to a slowly changing base potential. The time interval of each potential step in this series is ~40-50 ms. The current is measured at two time points of the pulse – first, just before the pulse starts and second when the pulse ends. The difference between the current values at these two points (δi) is plotted against the base potential. The resulting plot of δi vs. V is referred to as a differential pulse voltammogram consisting of current peak(s), the height of which is directly proportional to the concentration of the corresponding analyte(s). DPV offers an added advantage of lower charging current and allows measurements at concentrations as low as 10^{-8} M (Wang, J, 2006). This technique offers improved resolution for species with similar values of redox potentials and enables determination of very low concentrations of analytes. These advantages have rendered DPV highly suitable for applications involving the determination of analytes present at trace levels in given samples such as food. In other words, the most prominent application of DPV has been in the field of biosensing.

3.3 Experimental

3.3.1 Synthesis of yttria-zirconia-reduced graphene oxide (nY_2O_3-$nZrO_2$-rGO) nanocomposite

One step, hydrothermal method has been used for the synthesis of the nY_2O_3-$nZrO_2$-rGO nanocomposite. Briefly, 100 mg of GO was taken and homogenously dispersed in 20 ml of double distilled water by ultrasonication for 1 h. Similarly, zirconium ethoxide was separately dispersed in double distilled water (A) and NaOH was added to it dropwise followed by addition of CTAB. This reaction mixture was kept on stirring for 1 hr. Subsequently, a dispersion containing 0.01 M yttrium nitrate was prepared in double distilled water (B) and added to the zirconia precursor mixture A. This new reaction mixture was stirred at 200 rpm for 4 hr at room temperature, after which it was mixed with GO dispersion under constant stirring. The as-obtained black-colored mixture was transferred to a Teflon-lined stainless steel autoclave and keptat 170 ˚C for 17 h. Thereafter, it was allowed to cool at room temperature (~25 ˚C) yielding a greyish-black precipitate which was filtered and washed several times with deionized water and absolute ethanol till pH reached 7. The as-obtained filtered precipitate was then dried at 60 ˚C for 24 h to obtain the final product.

3.3.2 Functionalization of the nY_2O_3-$nZrO_2$-rGO nanocomposite

The as-synthesized nY_2O_3-$nZrO_2$-rGO nanocomposite was amine-functionalized using 3-aminopropyltriethyl silane (APTES). In brief, 100 mg of the nY_2O_3-$nZrO_2$-RGO nanocomposite was dispersed in a minimum amount of isopropanol and kept for 24 h on stirring (300 rpm; 25 ˚C) for maximal dispersion. Thereafter, 200 µL of 98% APTES was added to this dispersion followed by addition of 10 mL of water. Thus prepared reaction mixture was kept on stirring for 24-48 h (300 rpm; 25 ˚C) leading to the precipitation of the silanized nY_2O_3-$nZrO_2$-rGO nanocomposite. The thus functionalized APTES/nY_2O_3-$nZrO_2$-rGO nanocomposite was filtered and washed with distilled water (×5) and ethanol until the pH reached 7. The resulting product was dried at 60 ˚C and stored in dry conditions at room temperature till further use.

3.3.3 Electrophoretic deposition of APTES/nY_2O_3-$nZrO_2$-rGO nanocomposite

The functionalized nY_2O_3-$nZrO_2$-rGOnanocomposite was electrophoretically deposited on to a pre-hydrolyzed ITO electrode using the Genetix, GX3000C instrument. A homogenous dispersion of nY_2O_3-$nZrO_2$-rGO nanocomposite (0.2 mg mL^{-1}) was prepared in acetonitrile [C_2H_3N] and kept in an electrochemical glass cell. An ITO electrode and Pt wire were used as working electrode and auxillary electrode, respectively. A DC voltage of 45 V was applied for 180 s to this assembly resulting in the formation of thin films of the functionalized nY_2O_3-$nZrO_2$-rGO nanocomposite on to the ITO electrode.

3.3.4 Fabrication of the BSA/anti-CYFRA-21-1/APTES/nY_2O_3-$nZrO_2$-rGO/ITO immunoelectrode

A solution of anti-CYFRA-21-1 (50 µg mL^{-1}) was prepared in PBS (pH 7). 15 µL of this antibody solution was mixed with EDC and NHS in 2:1:1 ratio (final volume 30 µL). The resulting reaction mixture was incubated at room temperature for 20 min, and subsequently dropcasted on to the APTES/nY_2O_3-nZrO_2-rGO/ITO electrode in a uniform manner. Lastly, 30 μL of BSA (1 mg mL^{-1}) was used to block non-specific sites on the electrode. The thus fabricated BSA/anti-CYFRA-21-1/APTES/nY_2O_3-nZrO_2-rGO/ITO immunoelectrode was stored at 4 ˚C when not in use.

Chapter 4

Results and Discussion

4. Results and Discussion

4.1 Structural and morphological characterization

The phase composition of the hydrothermally synthesized nY_2O_3-$nZrO_2$-rGO nanocomposite has been analyzed through X-ray diffraction (XRD) in the range 30 ° - 70 ° (**Figure 4.1**). As shown in the **Figure**, the diffraction peaks occurring at diffraction angle (2Θ) of 30.4 °, 34.6 °, 50.2 ° and 59.8 ° correspond to the tetragonal phase of yttria-stabilized zirconia (JCPDS no. 83-0113). The maximum diffraction intensity has been found along the (002) plane indicating that crystal growth has preferentially occurred along this plane direction. The corresponding interplanar spacing (d_{002}) has been found to be 2.59 Å by the Bragg's equation given by –

$$n\lambda = 2d_{hkl}\sin\Theta \qquad \textbf{Eq. 4.1}$$

where, λ is the wavelength of source (1.5406 Å), n is the order (1) and Θ is the corresponding diffraction angle (0.3019 rad). Further, the peak observed at 24.3 ° can be attributed to the collective presence of (110) and (002) planes of monoclinic ZrO_2 and rGO, respectively (Kumar et al., 2015). This confirms the formation and grafting of nY_2O_3-$nZrO_2$ nanocomposite on to rGO surface.

The surface morphology of the synthesized nY_2O_3-$nZrO_2$-rGO nanocomposite and the fabricated APTES/nY_2O_3-$nZrO_2$-rGO/ITO and anti-CYFRA-21-1/APTES/nY_2O_3-$nZrO_2$-rGO/ITO electrodes has been studied via SEM analysis (**Figure 4.1(b-d)**). The sheet-like structure of rGO is clearly visible in **Figure 4.1(b)** which is decorated on the surface by flaky-appearing nY_2O_3-$nZrO_2$ nanocomposite. The surface of the APTES/nY_2O_3-$nZrO_2$/ITO appears rough, which may be due to the presence of bulky silane groups of APTES (**Figure 4.1(c)**).

However, in comparison, the surface roughness of the anti-CYFRA-21-1/APTES/nY_2O_3-nZrO_2-rGO/ITO electrode seems to be reduced considerably (**Figure 4.1(d)**). This decrease in roughness can be attributed to the uniform coverage of the APTES/nY_2O_3-nZrO_2-rGO/ITO electrode surface by anti-CYFRA-21-1 antibodies, which may have bound via APTES mediated conjugation.

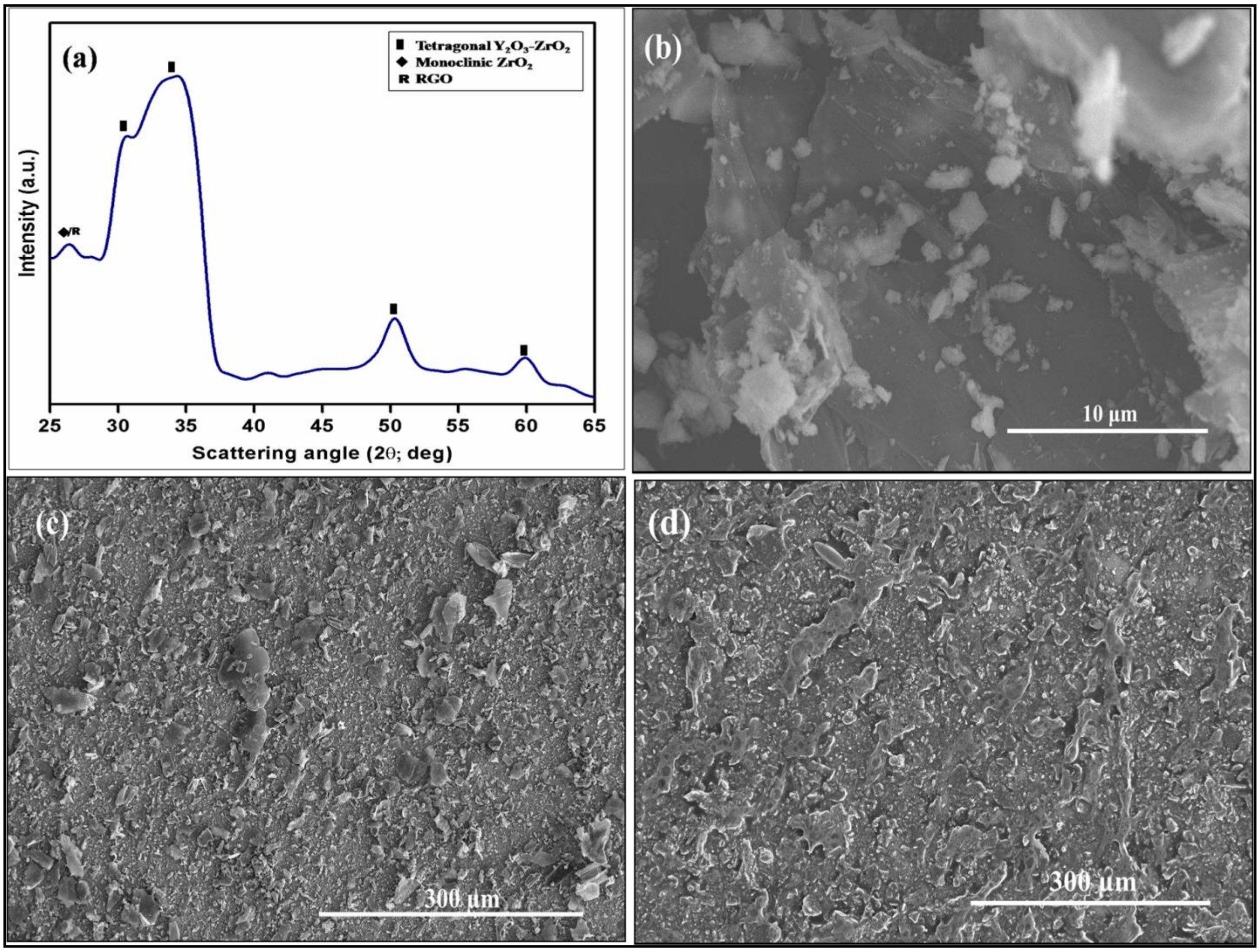

Figure 4.1 **(a)** X-ray diffraction pattern of the synthesized nY_2O_3-nZrO_2-rGO nanocomposite, and SEM micrographs of the **(b)** synthesized nY_2O_3-nZrO_2-rGO nanocomposite, **(c)** APTES/nY_2O_3-nZrO_2-rGO/ITO, and **(d)** anti-CYFRA-21-1/APTES/nY_2O_3-nZrO_2-rGO/ITO electrodes

4.2 FT-IR studies

The functional groups and bonds present in the APTES/nY_2O_3-nZrO_2-rGO/ITO and the anti-CYFRA-21-1/APTES/nY_2O_3-nZrO_2-rGO/ITO electrodes were analyzed via FT-IR studies

(**Figure 4.2**, **curves (a)** and **(b)**). The peaks between 400 – 480 cm^{-1} and 595 cm^{-1} correspond to the Zr(Y)-O vibrations of tetragonal yttria-stabilized zirconia (Phillippi et al., 1971). The peak at 1560 cm^{-1} corresponds to the bending vibration of N-H bonds (**Figure 4.2**, **curve (a)**), indicating the presence of free NH_2 groups of APTES on the electrode (Luo et al., 2008). The peaks at 2975 cm^{-1} and 3410 cm^{-1} correspond to N-H stretching and H-O-H vibrations, respectively. The peak at around 3800 cm^{-1} may correspond to both the Zr-OH vibrations and H-O-H vibrations. In comparison, an extra peak at 1644 cm^{-1} is evident in the spectra of the anti-CYFRA-21-1/APTES/nY_2O_3-nZrO_2-rGO/ITO electrode (**Figure 4.2, curve (b)**), which indicates the presence of amide C-N bond (N-H bend in primary amide) (Kumar et al., 2016). This confirms that anti-CYFRA-21-1 antibodies have been covalently immobilized on the electrode surface. Further, the peaks at 1073 cm^{-1}, 1247 cm^{-1} and 1472 cm^{-1} correspond to CH_2 scissoring vibrations and =C-H vibrations, respectively.

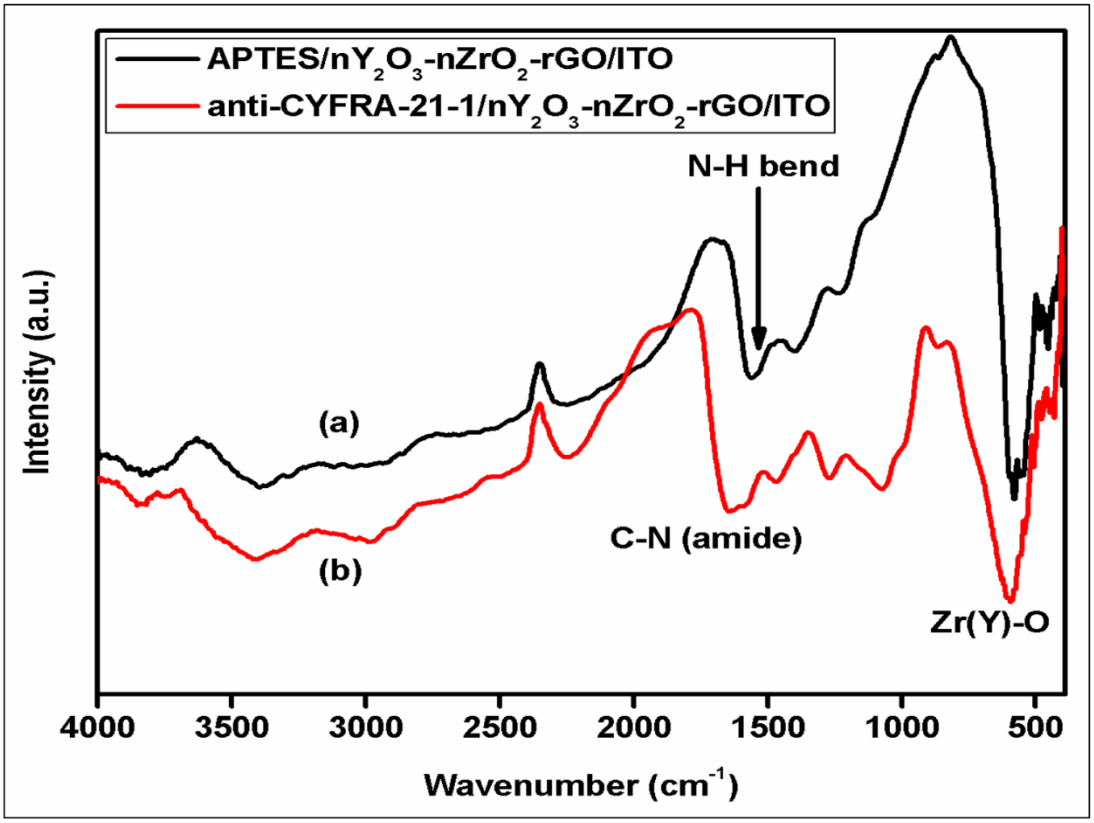

Figure 4.2 FT-IR spectra of the APTES/nY_2O_3-nZrO_2-rGO/ITO **(curve (a))** and the anti-CYFRA-21-1/APTES/nY_2O_3-nZrO_2-rGO/ITO **(curve (b))** electrodes

4.3 Electrochemical characterization

4.3.1 pH studies

The pH of the electrolyte affects the performance of a biosensor due to the pH-dependent activity of biomolecules. The effect of pH on the fabricated BSA/anti-CYFRA-21-1/APTES/nY_2O_3-nZrO_2-rGO/ITO immunoelectrode has been analyzed by differential pulse voltammetry (DPV) in PBS (50 mM) containing 5 mM $[Fe(CN)_6]^{3-/4-}$ and 0.9% NaCl (**Figure 4.3**). The results show considerable variations in the electrochemical response of the fabricated immunoelectrode within the pH range 6.0-8.0. The peak current response has been found to increase considerably when the pH was first increased from 6 to 7 pH units, whence it displayed the maximum response of 0.217 mA. Upon increasing the pH further, the response of the biosensor decreases significantly with the lowest value at pH 8. These results suggest that the activity of antibodies is maximum at pH 7. Thus, pH 7 has been chosen as the optimum pH for further experiments.

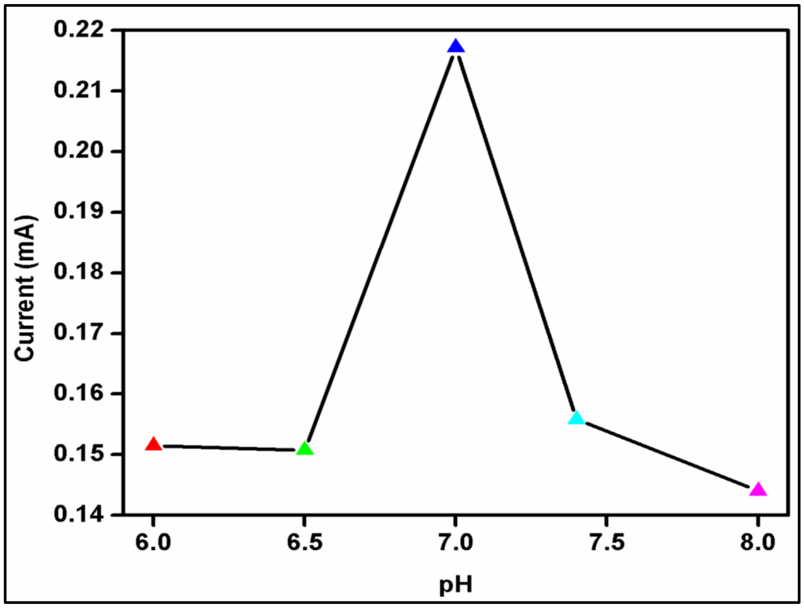

Figure 4.3 Electrochemical response of the BSA/anti-CYFRA-21-1/APTES/nY_2O_3-nZrO_2-rGO/ITO immunoelectrode as a function of pH

4.3.2 Electrode studies

The steps in the fabrication of the BSA/anti-CYFRA-21-1/APTES/nY_2O_3-nZrO_2-rGO/ITO biosensing platform have been characterized via DPV at a scan rate of 10 mV s^{-1} in PBS containing 5 mM $[Fe(CN)_6]^{3-/4-}$ and 0.9% NaCl (**Figure 4.5**). In general, the DPV curves of all the electrodes have been found symmetric in nature with the bare ITO showing a peak response of 0.3 mA (curve (i)). Upon deposition of the APTES/nY_2O_3-nZrO_2-rGO nanocomposite on to the ITO electrode, the magnitude of the peak response changed to 0.26 mA (curve (ii)). It is noteworthy that the peak response of the APTES/nY_2O_3-nZrO_2-rGO/ITO electrode has been found to be higher than that of the APTES/nY_2O_3/ITO electrode (0.25 mA; curve (iii)) indicating improved electrocatalytical behavior possibly due to addition of rGO (Shin et al., 2014). In addition, an increase of more than 2-fold has been found in the peak response of the APTES/nY_2O_3-nZrO_2-rGO/ITO in comparison to that of the APTES/nZrO_2-rGO/ITO electrode (0.1 mA; curve (vi)). This increase in the peak response can be attributed to the synergistic effect of the electrical conducting pathways made available by the rGO nanosheets and the high conductivity imparted by doping with Y_2O_3 (Shin et al., 2014). It has also been reported that YSZ thin films and nanocomposites exhibit excellent proton conduction via interfacial physisorped water molecules under humid conditions (Miyoshi et al., 2014; Scherrer et al., 2013). The oxygen vacancies present in the lattice of yttria-doped zirconia can also contribute, to a limited extent, to the enhanced conductivity (Scherrer et al., 2013).

The immobilization of anti-CYFRA-21-1 on to the APTES/nY_2O_3-nZrO_2-rGO/ITO electrode has been found to bring about a decrease in the peak response (0.24 mA; curve (iv)) This may be due to the masking of some of the charge conduction pathways by the globular antibodies. BSA immobilization has been carried out in order to block the non-specific sites at the electrode surface which led to an obvious decrease in the current response of the BSA/anti-CYFRA-21-1/APTES/nY_2O_3-nZrO_2-rGO/ITO immunoelectrode (0.22 mA; curve (v)).

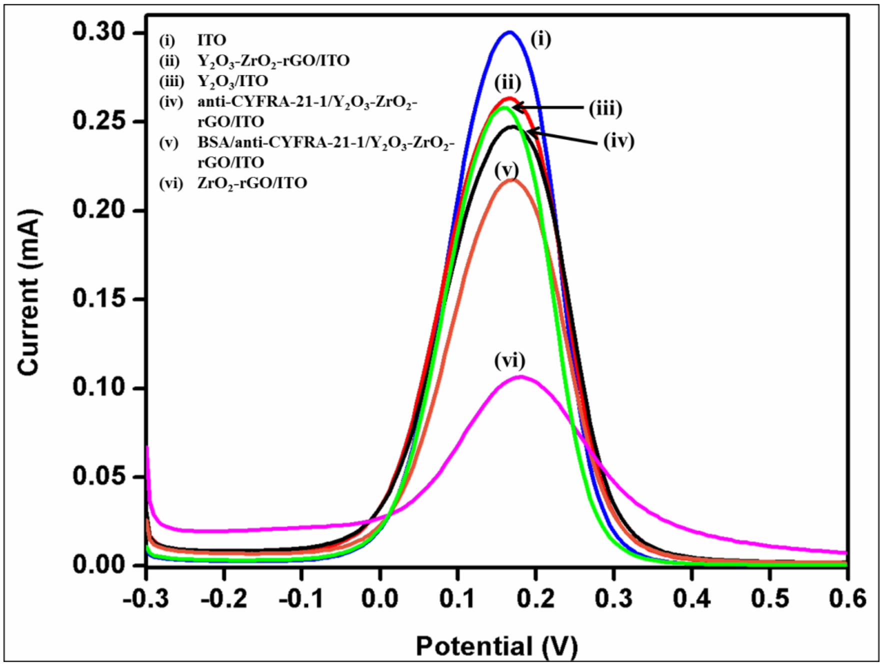

Figure 4.4 DPV curves of bare ITO (**curve (i)**), APTES/nY_2O_3-nZrO_2-rGO/ITO (**curve (ii)**), anti-CYFRA-21-1/APTES/nY_2O_3-nZrO_2-rGO/ITO (**curve (iii)**), BSA/anti-CYFRA-21-1/APTES/nY_2O_3-nZrO_2-rGO/ITO (**curve (iv)**), APTES/nY_2O_3/ITO (**curve (v)**) and APTES/nZrO_2-rGO/ITO (**curve (vi)**) as taken in PBS containing 5 mM $[Fe(CN)_6]^{3-/4-}$ and 0.9% NaCl

4.3.3 Scan rate studies

Cyclic voltammetric (CV) studies were conducted to investigate the response of the APTES/nY_2O_3-nZrO_2-rGO/ITO and BSA/anti-CYFRA-21-1/APTES/nY_2O_3-nZrO_2-rGO/ITO electrodes with increasing scan rate (40-150 mV s^{-1}) in PBS containing 5 mM $[Fe(CN)_6]^{3-/4-}$ and 0.9% NaCl (**Figure 4.6 (i)** and **4.6 (ii)**, respectively). A linear relationship ($R^2 = 0.99$) was found between the peak currents (I_{pc} and I_{pa}) and square root of scan rate (**inset (a)**) suggesting that the redox reaction is a diffusion-controlled process, wherein the redox species move to and from the redox centers at the BSA/anti-CYFRA-21-1/APTES/nY_2O_3-nZrO_2-rGO/ITO electrode surface (Kumar et al., 2015; Singh et al., 2013). A slight shift in the peak potential was observed with increasing scan rate indicating the quasi-reversibility of the redox reaction taking place at the electrode surface. However, the potential peak shift ($\Delta E_p = E_{pa} - E_{pc}$) was found to vary linearly ($R^2 = 0.99$) with square root of scan rate, indicating enhanced electrocatalytic behavior of the fabricated electrodes. The corresponding regression equations are given below.

$I_{pc(APTES/Y2O3\text{-}ZrO2\text{-}rGO/ITO)} = 0.08\ \text{mA}\ (\text{mV s}^{-1})^{-1/2} \times \text{scan rate}\ (\text{mV s}^{-1})^{1/2} + 0.174\ \text{mA},$

$R^2 = 0.995$ **Eq. 4.2**

$I_{pa(APTES/Y2O3\text{-}ZrO2\text{-}rGO/ITO)} = -\ 0.059\ \text{mA}\ (\text{mV s}^{-1})^{-1/2} \times \text{scan rate}\ (\text{mV s}^{-1})^{1/2} - 0.254\ \text{mA},$

$R^2 = 0.995$ **Eq. 4.3**

$I_{pc(BSA/anti\text{-}CYFRA\text{-}21\text{-}1/APTES/Y2O3\text{-}ZrO2\text{-}rGO/ITO)} = 0.069\ \text{mA}\ (\text{mV s}^{-1})^{-1/2} \times [\text{scan rate}\ (\text{mV s}^{-1})]^{1/2}$

$+ 0.177\ \text{mA},$ $R^2 = 0.999$ **Eq. 4.4**

$I_{pa(BSA/anti\text{-}CYFRA\text{-}21\text{-}1/APTES/Y2O3\text{-}ZrO2\text{-}rGO/ITO)} = -\ 0.055\ \text{mA}\ (\text{mV s}^{-1})^{-1/2} \times [\text{scan rate}\ (\text{mV s}^{-1})]^{1/2}$

$- 0.201\ \text{mA},$ $R^2 = 0.997$ **Eq. 4.5**

$\Delta E_p\ (\text{V})_{APTES/Y2O3\text{-}ZrO2\text{-}rGO/ITO} = 0.013\ \text{V}\ (\text{mV s}^{-1})^{-1/2} \times [\text{scan rate}\ (\text{mV s}^{-1})]^{1/2} + 0.105\ \text{V},$

$R^2 = 0.996$ **Eq. 4.6**

$\Delta E_p\ (\text{V})_{BSA/anti\text{-}CYFRA\text{-}21\text{-}1/APTES/Y2O3\text{-}ZrO2\text{-}rGO/ITO} = -0.015\ \text{V}\ (\text{mV s}^{-1})^{-1/2} \times [\text{scan rate}\ (\text{mV s}^{-1})]^{1/2}$

$+ 0.109\ \text{V},$ $R^2 = 0.994$ **Eq. 4.7**

The magnitudes of the diffusion coefficient for the APTES/nY_2O_3-nZrO_2-rGO/ITO and the BSA/anti-CYFRA-21-1/APTES/nY_2O_3-nZrO_2-rGO/ITO electrodes were found to be 1.72×10^{-13} $\text{cm}^2\ \text{s}^{-1}$ and 1.36×10^{-13} $\text{cm}^2\ \text{s}^{-1}$, respectively using the Randles-Sevcik's equation given as:

$$I_p = (2.69 \times 10^5)\, n^{3/2} A D^{1/2} C v^{1/2} \qquad \textbf{Eq. 4.8}$$

where, I_p is the peak current, n is the no. of electrons (= 1), A is the effective surface area (= 0.25 cm^2), D is the diffusion coefficient, C is the concentration of the redox species (= 5 mM) and v is the scan rate.

The charge transfer rate constant (K_s) is also an important electrode parameter which determines the rate of charge transfer across the electrode surface. The K_s values were determined by the following equation –

$$K_s = mnFv/RT \qquad \textbf{Eq. 4.9}$$

where, m is the peak-to-peak difference (V), n is the number of electrons (1), F is Faraday's constant (96, 485 C mol^{-1}), v is the scan rate (50 mV s^{-1}), R is the gas constant (8.314 J mol^{-1} K^{-1}) and T is the temperature (298 K). The magnitude of K_s was found to increase from 0.385s^{-1} for the APTES/nY_2O_3-nZrO_2-rGO/ITO electrode to 0.418 s^{-1} for the BSA/anti-CYFRA-21-1/APTES/nY_2O_3-nZrO_2-rGO/ITO immunoelectrode. This increase in the K_s can be attributed to the oriented immobilization of antibodies on the immunoelectrode surface that provides a faster route for electron transfer across the electrode surface (Singh et al., 2013). Further, the surface concentration of electroactive species has been calculated using the Brown-Anson model –

$$I_p = n^2F^2\gamma Av/4RT \qquad \textbf{Eq. 4.10}$$

where, I_p is the peak current, n is the no. of electrons (1), F is Faraday's constant (96 485 C mol^{-1}), γ is concentration of electroactive species, A is the effective electrode surface area (0.25 cm^2), v is scan rate, R is gas constant (8.314 J mol^{-1} K^{-1}) and T is temperature (298 K). The surface concentration for the APTES/nY_2O_3-nZrO_2-rGO/ITO (6.35 × 10^{-8}mol cm^{-2}) has been found to be higher than that of the BSA/anti-CYFRA-21-1/APTES/nY_2O_3-nZrO_2-rGO/ITO immunoelectrode (5.65×10^{-8} mol cm^{-2}). This may be due to the masking of electroactive sites after immobilization of biomolecules on to the APTES/nY_2O_3-nZrO_2-rGO/ITO electrode surface.

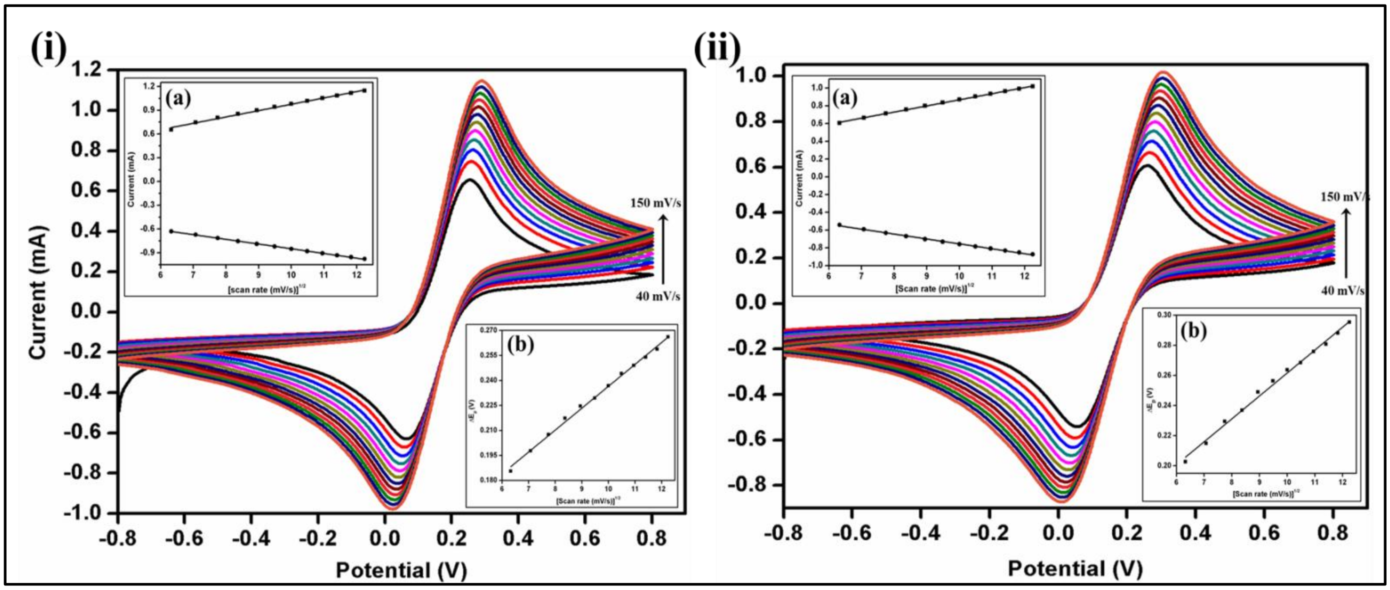

Figure 4.5 CV curves of **(i)** APTES/nY_2O_3-nZrO_2-rGO/ITO, and **(ii)** BSA/anti-CYFRA-21-1/APTES/nY_2O_3-nZrO_2-rGO/ITO electrodes as a function of scan rate (40-150 mV/s); **inset (a)** redox peak current (I_p) as a function of square root of the scan rate ($v^{1/2}$); **inset (b)** peak potential shift (ΔE_p) as a function of square root of the scan rate ($v^{1/2}$)

4.4 Incubation time studies

The incubation time given for the formation of antigen-antibody complex at the biosensing interface is critical to the electrochemical response of the biosensor. **Figure 4.6** shows the results of DPV studies conducted to determine the optimum incubation time for the response of the fabricated BSA/anti-CYFRA-21-1/APTES/nY_2O_3-nZrO_2-rGO/ITO biosensor towards CYFRA-21-1 antigen (2 ng mL^{-1}). It was observed that the peak response of the biosensor displays a somewhat erratic behavior up to 15 min, after which it attained a stable value of 0.21 mA. This suggests that 15 min is the optimum time required for the complete binding of the CYFRA-21-1 antigen with the antibodies present on the biosensing surface. Incubation for more than 15 min did not bring any significant change in the biosensor response possibly due to the saturation of binding sites and/or binding of all CYFRA-21-1 present in the electrolyte with the antibodies. Thus, 15 min has been chosen as the incubation time for response studies.

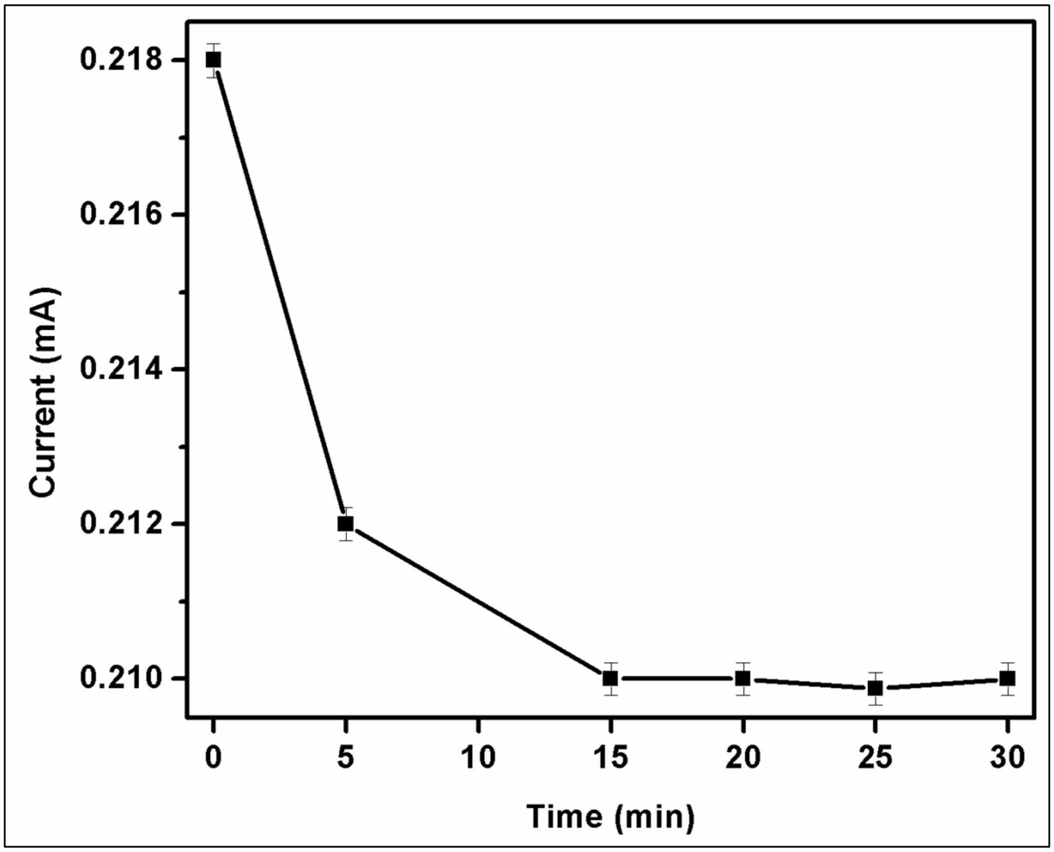

Figure 4.6 Response of the fabricated BSA/anti-CYFRA-21-1/APTES/nY_2O_3-nZrO_2-rGO/ITO immunoelectrode to CYFRA-21-1 (2 ng mL^{-1}) as a function of time

4.5 Electrochemical response studies

The change in the electrochemical response of the fabricated BSA/anti-CYFRA-21-1/APTES/nY_2O_3-nZrO_2-rGO/ITO biosensor with increasing concentration of CYFRA-21-1 has been analyzed via DPV in PBS containing $[Fe(CN)_6]^{3-/4-}$ (5 mM) and 0.9% NaCl at a scan rate of 10 mV s^{-1} (**Figure 4.7(a)**). It was observed that increase in the CYFRA-21-1 concentration results in a corresponding decrease in the peak current of the biosensor. This decrease in the current might be attributed to the interaction of bulky CYFRA-21-1 molecules with the anti-CYFRA-21-1 antibodies, resulting in the blocking of charge conduction pathways at the BSA/anti-CYFRA-21-1/APTES/nY_2O_3-nZrO_2-rGO/ITO biosensing surface. The corresponding calibration curve revealed the linear dependence of the biosensor's peak current with CYFRA-21-1 concentration (**Figure 4.7(b)**). The corresponding regression equation is given by –

I_p (mA) = - 2.4 μA mL ng^{-1} × concentration (ng mL^{-1}) + 214.9 μA,

$R^2 = 0.983$ **Eq. 4.11**

The linear range of the biosensor has been found to be 0.25 – 22 ng mL^{-1} which sufficiently covers the entire physiological range of CYFRA-21-1. In addition, the biosensor displayed an excellent sensitivity of 9.6 μA mL ng^{-1} cm^{-2} which is much superior to the previously reported biosensors for CYFRA-21-1 detection. The detection limit, as evaluated by $3\sigma/m$, was determined to be 0.1 ng mL^{-1}, where σ is the standard deviation in the electrochemical response and m is the slope (or, sensitivity) of the fabricated BSA/anti-CYFRA-21-1/APTES/nY_2O_3-nZrO_2-rGO/ITO biosensor.

A control experiment was conducted to determine the electrochemical response of the APTES/nY_2O_3-nZrO_2-rGO/ITO electrode as a function of CYFRA-21-1 concentration (0 – 22 ng mL^{-1}) (**Figure 4.7 (c)**).No significant change in the current response of the APTES/nY_2O_3-nZrO_2-rGO/ITO electrode has been found even at higher concentrations of CYFRA-21-1 revealing that change in the electrochemical response of the BSA/anti-CYFRA-21-1/APTES/nY_2O_3-nZrO_2-rGO/ITO electrode is solely due to antibody-antigen interactions.

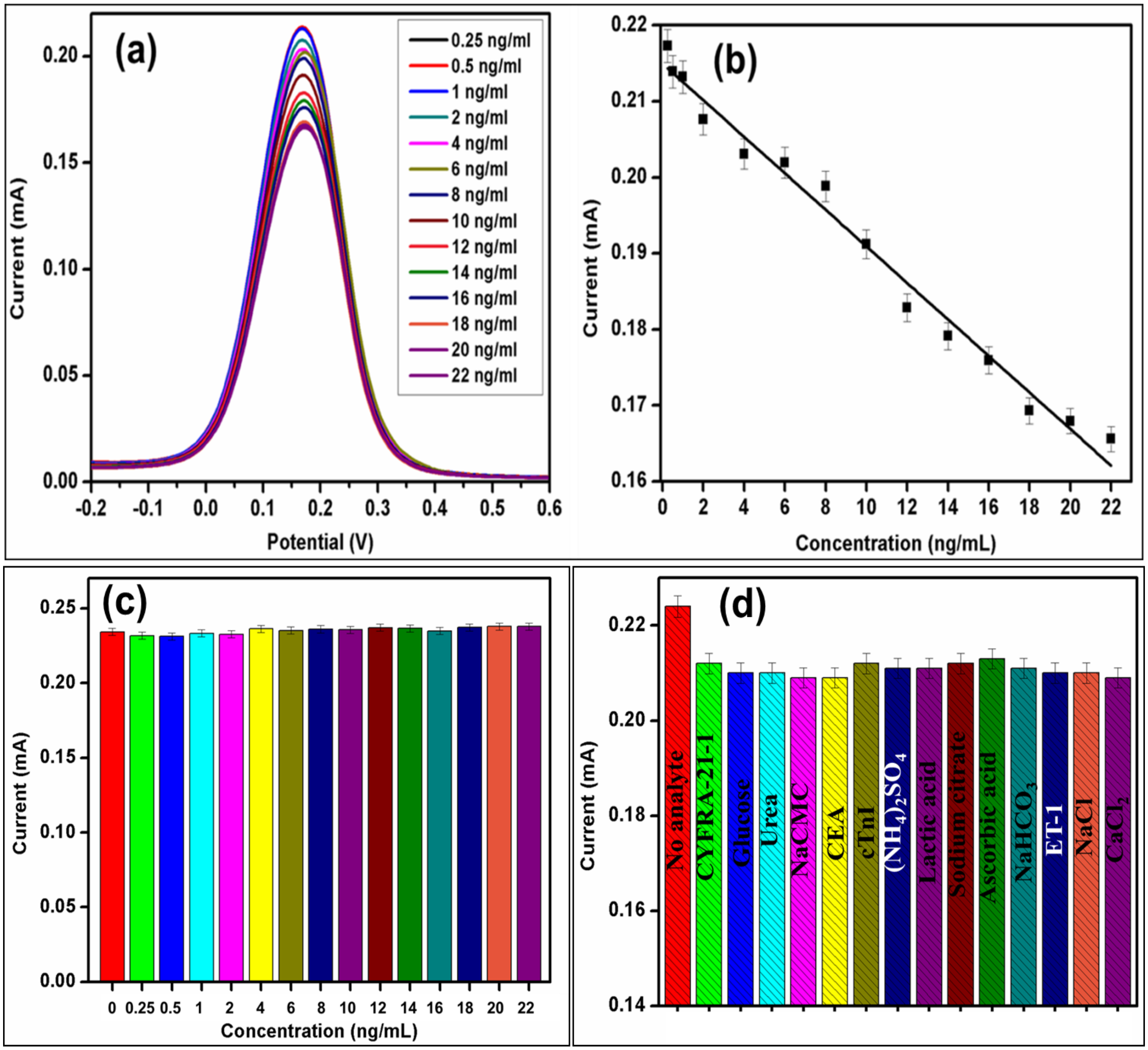

Figure 4.7 **(a)** DPV curves of the BSA/anti-CYFRA-21-1/APTES/nY_2O_3-nZrO_2-rGO/ITO immunoelectrode as a function of CYFRA-21-1 concentration (0.25-22 ng mL^{-1}), **(b)** calibration plot derived from DPV curves of BSA/anti-CYFRA-21-1/APTES/nY_2O_3-nZrO_2-rGO/ITO immunoelectrode as a function of CYFRA-21-1 concentration (0.25-22 ng mL^{-1}), **(c)** electrochemical response of the APTES/nY_2O_3-nZrO_2-rGO/ITO electrode as a function of increasing CYFRA-21-1 concentration (0.25-22 ng mL^{-1}), and **(d)** peak current response of the BSA/anti-CYFRA-21-1/APTES/nY_2O_3-nZrO_2-rGO/ITO in the presence of CYFRA-21-1 (2 ng mL^{-1}) and other common interferents found in saliva.

4.6 Interferent analysis, thermal stability and shelf life study

The variation in the electrochemical response of the fabricated BSA/anti-CYFRA-21-1/APTES/nY_2O_3-nZrO_2-rGO/ITO biosensor in the presence of common interfering agents has also been investigated via DPV studies (**Figure 4.7 (d)**). The response of the biosensor was first recorded in the presence of CYFRA-21-1antigen (2 ng mL^{-1}) (0.21 mA; %RSD – 1%). Thereafter, equal amounts of different interferents were added in a sequential manner in their normal physiological range in saliva, such as glucose (7 mg mL^{-1}), urea (1 mg mL^{-1}), sodium carboxymethylcellulose (NaCMC; 10 mg mL^{-1}), CEA (4 – 16 ng mL^{-1}), cardiac troponin I (cTnI; 0.19 ng mL^{-1}), ammonium sulphate ($(NH_4)_2SO_4$; 0.3 mg mL^{-1}), lactic acid (0.03 µg mL^{-1}), sodium citrate (5 µg mL^{-1}), ascorbic acid (0.24 µg mL^{-1}), sodium bicarbonate ($NaHCO_3$; 0.1 mg mL^{-1}), endothelin-1 (ET-1; 1 pg mL^{-1}), NaCl (20 mM), and $CaCl_2$ (8.38 mM). The addition of cTnI, $(NH_4)_2SO_4$, lactic acid, Na citrate and $NaHCO_3$ yielded no significant change (0 – 0.5%) in the peak response of the fabricated biosensor, while a small change (~ 1%) was found in the peak response upon the addition of remaining interferents. It reveals that the fabricated BSA/anti-CYFRA-21-1/APTES/nY_2O_3-nZrO_2-rGO/ITO remains largely unaffected by the presence of interferents and has potential for practical applicability.

The effect of temperature (20 – 65 ˚C) on the electrochemical response of the APTES/nY_2O_3-nZrO_2-rGO/ITO and APTES/nZrO_2-rGO/ITO electrodes has been studied via DPV in PBS buffer (pH 7) supplemented with 5 mM $[Fe(CN)_6]^{3-/4-}$ (**Figure 4.8**). A continual increase in the peak response of both the electrodes has been observed till 50 ˚C. Thereafter, while the APTES/nY_2O_3-nZrO_2-rGO/ITO electrode displayed a small but gradual decrease in the peak response (**Figure 4.8**, **curve (i)**), the peak response of the APTES/nZrO_2-rGO/ITO electrode (**Figure 4.8**, **curve (ii)**) electrode was found to reduce continually at temperatures above 55 ˚C. The APTES/nY_2O_3-nZrO_2-rGO/ITO electrode displayed 3% reduction in its peak current compared to 7% reduction shown by the APTES/nZrO_2-rGO/ITO electrode. It is noteworthy that the peak response of the APTES/nY_2O_3-nZrO_2-rGO/ITO electrode remained higher than that of the APTES/nZrO_2-rGO/ITO electrode at all temperatures. This suggests that Y_2O_3 plays a role in the sustained peak response and enhanced electrochemical activity of the APTES/nY_2O_3-nZrO_2-rGO/ITO electrode at all temperatures.

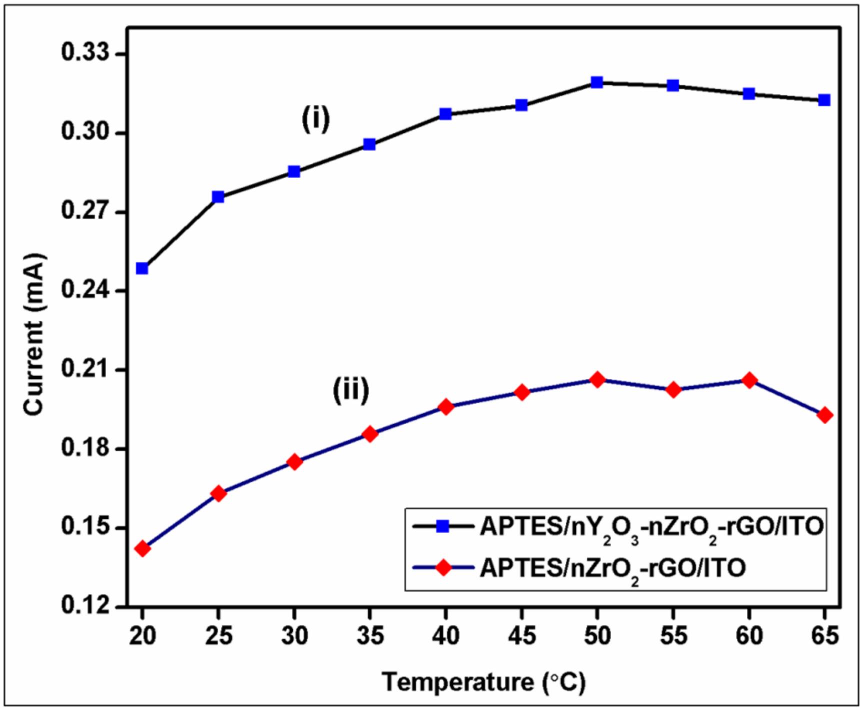

Figure 4.8 Electrochemical response of the APTES/nY_2O_3-nZrO_2-rGO/ITO and the APTES/nZrO_2-rGO/ITO electrodes as a function of temperature

The stability of the fabricated BSA/anti-CYFRA-21-1/APTES/nY_2O_3-nZrO_2-rGO/ITO biosensor has been determined by measuring its electrochemical response in the presence of standard CYFRA-21-1 solution (2 ng mL^{-1}) in PBS buffer (pH 7) containing 5 mM $[Fe(CN)_6]^{3-/4-}$ at a regular interval of 7 days (**Figure 4.9**). The biosensor retained 83% of its original peak response even after 14 days of operation. A gradual but continual decrease was observed thereafter. The peak response reached 66% of its original value by the 9th week. This decrease might be due to reduction in the thickness of the APTES/nY_2O_3-nZrO_2-rGO thin films.

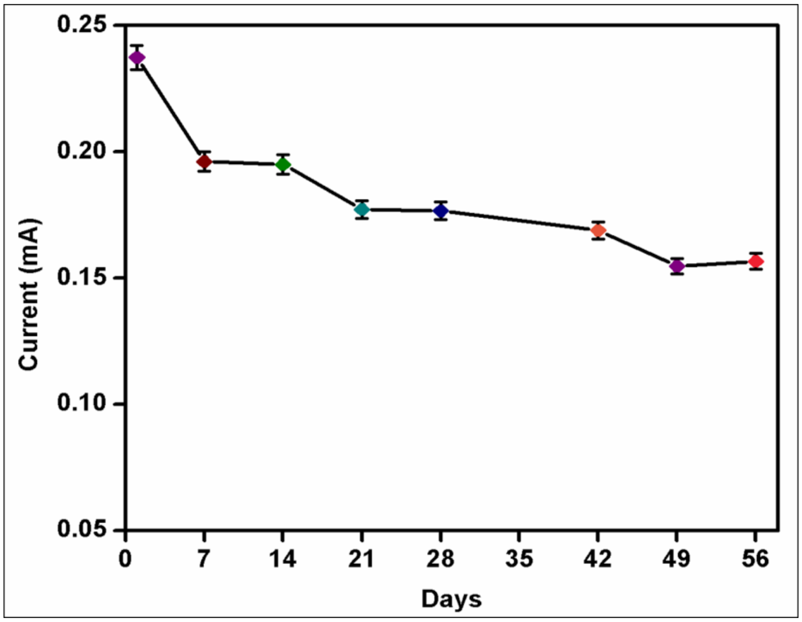

Figure 4.9 Shelf life studies of BSA/anti-CYFRA-21-1/nY_2O_3-nZrO_2-rGO/ITO immunoelectrode

Platform	**Biomarker**	**Technique used**	**Linear detection range (LOD)**	**Sensitivity**	**Response time**	**Reference**
Endonuclease target recycling amplification	ORAOV1	DPV	1 pM – 10 pM (0.35 pM)	5.4014×10^{-3} µA pM^{-1}	30 min	Tan et al. 2015
Magnet-controllable gold electrode	has-miR-200a	Chronoamperometry	1 aM – 10 fM (0.22 aM)	0.4608 µA aM^{-1}	-	Wang et al. 2013
ZrO_2-based immunosensor	CYFRA-21-1	DPV	2-16 ng mL^{-1} (0.08 ng mL^{-1})	2.2 mA mL ng^{-1}	20 min	Kumar et al. 2015
HfO_2-based immunosensor	CYFRA-21-1	CV	2-18 ng mL^{-1} (0.21 ng mL^{-1})	9.28 µA mL ng^{-1} cm^{-2}	15 min	Kumar et al. 2016
ZrO_2-rGO-based immunosensor	CYFRA-21-1	DPV	2-22 ng mL^{-1} (0.122 ng mL^{-1})	0.756 µA mL ng^{-1}	16 min	Kumar et al. 2016
Y_2O_3-ZrO_2-rGO-based immunosensor	CYFRA-21-1	DPV	0.25 – 22 ng mL^{-1} (0.1 ng mL^{-1})	9.6 µA mL ng^{-1} cm^{-2}	15 min	Present work

Table 4.1 Biosensors for oral cancer detection

Chapter 5

Conclusions

5. Conclusions

We have fabricated an efficient biosensing platform based on a nanocomposite consisting of rGO nanosheets decorated with yttria-stabilized zirconia nanoparticles (nY_2O_3-$nZrO_2$-rGO) for the detection of oral cancer biomarker CYFRA-21-1 in human saliva. nY_2O_3-$nZrO_2$-rGO nanocomposite was synthesized hydrothermally and silanized via APTES for grafting of amine groups. Thereafter, the functionalized APTES/nY_2O_3-$nZrO_2$-rGO nanocomposite was electrophoretically deposited on to ITO electrodes. anti-CYFRA-21-1 antibodies were covalently immobilized on to the APTES/nY_2O_3-$nZrO_2$-rGO/ITO electrode and BSA was used for blocking of non-specific sites. DPV studies demonstrated that the APTES/nY_2O_3-$nZrO_2$-rGO/ITO electrode possesses superior electrochemical activity in comparison to the APTES/nY_2O_3/ITO and APTES/$nZrO_2$-rGO/ITO electrodes. The fabricated BSA/anti-CYFRA-21-1/APTES/nY_2O_3-$nZrO_2$-rGO/ITO biosensor efficiently detected CYFRA-21-1, a salivary oral cancer biomarker, in a wide linear range of 0.25 – 22 ng mL^{-1} with notable sensitivity of 9.6 µA mL ng^{-1} cm^{-2} and detection limit of 0.1 ng mL^{-1}. Our study is the first to demonstrate that nY_2O_3-$nZrO_2$-rGO nanocomposite can be efficiently utilized to fabricate a sensitive, label-free electrochemical biosensing platform for diagnostic purposes.

Chapter 6

Future Perspectives

6. Future Perspectives

Nanomaterials hold much potential in the development of a new generation of biosensors for diagnostic applications. The catalytic properties of nanomaterials coupled with the novel detection methodologies such as electrochemical, surface enhanced resonance spectroscopy, and field effect transistors, etc. hold enough potential to surpass traditional techniques such as ELISA, microarrays, and nuclear magnetic resonance (Mannoor et al., 2012). Recently developed, the *in vitro* biosensors with detection limits at the femtomolar and attomolar levels demonstrate higher sensitivity than traditional techniques (Tan et al., 2013). The specificity of such devices using nanowires and microfluidic channels also exceeds the traditional methods as they are able to differentiate single mismatch nucleic acid base pairs. In addition, these systems offer rapid detection of target analytes and low-cost analysis due to minimal use of reagents (Kumar et al., 2012; Wang 2006). There have been a few reports wherein YSZ has been used in wireless sensing. This can potentially be useful in diagnostics, particularly in the development of *in vivo* biosensors coupled with wireless telemetry systems, such as Bluetooth, etc. In addition, scaffolds incorporated with YSZ have been reported to be highly conducive to bone growth. This distinctive feature may help in developing flexible, wearable smart nanodevices that would be capable of both diagnostics and therapeutics applications. A few *in vivo* biosensors have demonstrated the quantitative detection of salivary biomarkers such as metabolites and proteins (Chang et al., 2015; Chang et al. 2014; Mannoor et al., 2012). We believe that integration of the existing sensing mechanisms of salivary biomarkers with the emerging flexible electronic technologies, miniaturized wireless telemetry systems, and advanced soft materials will open a new era for wearable, *in vivo* salivary diagnostic devices.

Chapter 7

References

7. References

Afsharmanesh, E., Karimi-Maleh, H., Pahlavan, A., Vahedi, J., 2013. Electrochemical behavior of morphine at ZnO/CNT nanocomposite room temperature ionic liquid modified carbon paste electrode and its determination in real samples. Journal of Molecular Liquids 181, 8-13.

Ali, M.A., Singh, C., Mondal, K., Srivastava, S., Sharma, A., Malhotra, B.D., 2016. Mesoporous Few-Layer Graphene Platform for Affinity Biosensing Application. ACS applied materials & interfaces 8(12), 7646-7656.

Awan, K., Morgan, P., Warnakulasuriya, S., 2011. Evaluation of an autofluorescence based imaging system (VELscope™) in the detection of oral potentially malignant disorders and benign keratoses. Oral oncology 47(4), 274-277.

Bano, S., David, M.P., Indira, A., 2015. Salivary Biomarkers for Oral Squamous Cell Carcinoma: An Overview.

Barak, V., Meirovitz, A., Leibovici, V., Rachmut, J., Peretz, T., Eliashar, R., Gross, M., 2015. The Diagnostic and Prognostic Value of Tumor Markers (CEA, SCC, CYFRA 21-1, TPS) in Head and Neck Cancer Patients. Anticancer Research 35(10), 5519-5524.

Besteman, K., Lee, J.-O., Wiertz, F.G., Heering, H.A., Dekker, C., 2003. Enzyme-coated carbon nanotubes as single-molecule biosensors. Nano letters 3(6), 727-730.

Binnie, V., McHugh, S., Macpherson, L., Borland, B., Moir, K., Malik, K., 2004. The validation of self-reported smoking status by analysing cotinine levels in stimulated and unstimulated saliva, serum and urine. Oral diseases 10(5), 287-293.

Bitounis, D., Ali-Boucetta, H., Hong, B.H., Min, D.H., Kostarelos, K., 2013. Prospects and challenges of graphene in biomedical applications. Advanced Materials 25(16), 2258-2268.

Boffetta, P., Hecht, S., Gray, N., Gupta, P., Straif, K., 2008. Smokeless tobacco and cancer. The Lancet Oncology 9(7), 667-675.

Brailo, V., Vucicevic-Boras, V., Lukac, J., Biocina-Lukenda, D., Zilic-Alajbeg, I., Milenovic, A., Balija, M., 2012. Salivary and serum interleukin 1 beta, interleukin 6 and tumor necrosis factor alpha in patients with leukoplakia and oral cancer. Med Oral Patol Oral Cir Bucal 17(1), e10-e15.

Braun, P.V., 2003. and Biologically Inspired Nanocomposites. PM Ajayan, LS Schadler, PV Braun, 155.

Cardoso, A.R., Moreira, F.T., Fernandes, R., Sales, M.G.F., 2016. Novel and simple electrochemical biosensor monitoring attomolar levels of miRNA-155 in breast cancer. Biosensors and Bioelectronics 80, 621-630.

Chan, R.N., Stoner, B.R., Thompson, J.Y., Scattergood, R.O., Piascik, J.R., 2013. Fracture toughness improvements of dental ceramic through use of yttria-stabilized zirconia (YSZ) thin-film coatings. Dental materials 29(8), 881-887.

Cheng, Y.-S.L., Rees, T., Wright, J., 2014. A review of research on salivary biomarkers for oral cancer detection. Clinical and translational medicine 3(1), 1.

Chikkaveeraiah, B.V., Bhirde, A.A., Morgan, N.Y., Eden, H.S., Chen, X., 2012. Electrochemical immunosensors for detection of cancer protein biomarkers. ACS nano 6(8), 6546-6561.

Chung, C., Kim, Y.-K., Shin, D., Ryoo, S.-R., Hong, B.H., Min, D.-H., 2013. Biomedical applications of graphene and graphene oxide. Accounts of chemical research 46(10), 2211-2224.

Compton, O.C., Nguyen, S.T., 2010. Graphene Oxide, Highly Reduced Graphene Oxide, and Graphene: Versatile Building Blocks for Carbon-Based Materials. small 6(6), 711-723.

Crespilho, F.N., Lanfredi, A.J., Leite, E.R., Chiquito, A.J., 2009. Development of individual semiconductor nanowire for bioelectrochemical device at low overpotential conditions. Electrochemistry Communications 11(9), 1744-1747.

Das, B.R., Nagpal, J.K., 2002. Understanding the biology of oral cancer. Medical Science Monitor 8(11), RA258-RA267.

Doria, G., Conde, J., Veigas, B., Giestas, L., Almeida, C., Assunção, M., Rosa, J., Baptista, P.V., 2012. Noble metal nanoparticles for biosensing applications. Sensors 12(2), 1657-1687.

El-Sayed, I.H., Huang, X., El-Sayed, M.A., 2005. Surface plasmon resonance scattering and absorption of anti-EGFR antibody conjugated gold nanoparticles in cancer diagnostics: applications in oral cancer. Nano letters 5(5), 829-834.

Elashoff, D., Zhou, H., Reiss, J., Wang, J., Xiao, H., Henson, B., Hu, S., Arellano, M., Sinha, U., Le, A., 2012. Prevalidation of salivary biomarkers for oral cancer detection. Cancer Epidemiology Biomarkers & Prevention 21(4), 664-672.

Erdem, A., 2007. Nanomaterial-based electrochemical DNA sensing strategies. Talanta 74(3), 318-325.

Fan, Z., Senapati, D., Singh, A.K., Ray, P.C., 2012. Theranostic magnetic core–plasmonic shell star shape nanoparticle for the isolation of targeted rare tumor cells from whole blood, fluorescence imaging, and photothermal destruction of cancer. Molecular pharmaceutics 10(3), 857-866.

Feng, L., Chen, Y., Ren, J., Qu, X., 2011. A graphene functionalized electrochemical aptasensor for selective label-free detection of cancer cells. Biomaterials 32(11), 2930-2937.

Ferlay, J., Soerjomataram, I., Dikshit, R., Eser, S., Mathers, C., Rebelo, M., Parkin, D.M., Forman, D., Bray, F., 2015. Cancer incidence and mortality worldwide: sources, methods and major patterns in GLOBOCAN 2012. International journal of cancer 136(5), E359-E386.

Feynman, R.P., 1960. There's plenty of room at the bottom. Engineering and science 23(5), 22-36.

Fornabaio, M., Palmero, P., Traverso, R., Esnouf, C., Reveron, H., Chevalier, J., Montanaro, L., 2015. Zirconia-based composites for biomedical applications: Role of second phases on composition, microstructure and zirconia transformability. Journal of the European Ceramic Society 35(14), 4039-4049.

Giovannacci, I., Vescovi, P., Manfredi, M., Meleti, M., 2016. Non-invasive visual tools for diagnosis of oral cancer and dysplasia: A systematic review. Medicina oral, patologia oral y cirugia bucal 21(3), e305.

Gómez-Navarro, C., Meyer, J.C., Sundaram, R.S., Chuvilin, A., Kurasch, S., Burghard, M., Kern, K., Kaiser, U., 2010. Atomic structure of reduced graphene oxide. Nano letters 10(4), 1144-1148.

Holzinger, M., Le Goff, A., Cosnier, S., 2014. Nanomaterials for biosensing applications: a review. Frontiers in chemistry 2.

Jablonska, E., Piotrowski, L., Grabowska, Z., 1997. Serum Levels of IL-lβ, IL-6, TNF-α, sTNF-RI and CRP in Patients with oral cavity cancer. Pathology & Oncology Research 3(2), 126-129.

Jang, D.Y., Kim, H.K., Kim, J.W., Bae, K., Schlupp, M.V., Park, S.W., Prestat, M., Shim, J.H., 2015. Low-temperature performance of yttria-stabilized zirconia prepared by atomic layer deposition. Journal of Power Sources 274, 611-618.

Jessie, K., Jayapalan, J.J., Ong, K.C., Rahim, A., Haji, Z., Zain, R.M., Wong, K.T., Hashim, O.H., 2013. Aberrant proteins in the saliva of patients with oral squamous cell carcinoma. Electrophoresis 34(17), 2495-2502.

Jiang, H., Ma, J., Li, C., 2012. Mesoporous carbon incorporated metal oxide nanomaterials as supercapacitor electrodes. Advanced Materials 24(30), 4197-4202.

Jiang, L., Gu, S., Ding, Y., Jiang, F., Zhang, Z., 2014. Facile and novel electrochemical preparation of a graphene–transition metal oxide nanocomposite for ultrasensitive electrochemical sensing of acetaminophen and phenacetin. Nanoscale 6(1), 207-214.

Jin, B., Wang, P., Mao, H., Hu, B., Zhang, H., Cheng, Z., Wu, Z., Bian, X., Jia, C., Jing, F., 2014. Multi-nanomaterial electrochemical biosensor based on label-free graphene for detecting cancer biomarkers. Biosensors and Bioelectronics 55, 464-469.

Johnson, N.W., Warnakulasuriya, S., Gupta, P., Dimba, E., Chindia, M., Otoh, E., Sankaranarayanan, R., Califano, J., Kowalski, L., 2011. Global oral health inequalities in incidence and outcomes for oral cancer causes and solutions. Advances in dental research 23(2), 237-246.

Kang, D., Vallée-Bélisle, A., Porchetta, A., Plaxco, K.W., Ricci, F., 2012. Re-engineering Electrochemical Biosensors To Narrow or Extend Their Useful Dynamic Range. Angewandte Chemie International Edition 51(27), 6717-6721.

Kanniyappan, U., Prakasarao, A., Dornadula, K., Singaravelu, G., 2016. An in vitro diagnosis of oral premalignant lesion using time-resolved fluorescence spectroscopy under UV excitation—a pilot study. Photodiagnosis and photodynamic therapy 14, 18-24.

Khan, M., Tahir, M.N., Adil, S.F., Khan, H.U., Siddiqui, M.R.H., Al-warthan, A.A., Tremel, W., 2015. Graphene based metal and metal oxide nanocomposites: synthesis, properties and their applications. Journal of Materials Chemistry A 3(37), 18753-18808.

Khariwala, S.S., Carmella, S.G., Stepanov, I., Fernandes, P., Lassig, A.A., Yueh, B., Hatsukami, D., Hecht, S.S., 2013. Elevated levels of 1-hydroxypyrene and N′-nitrosonornicotine in smokers with head and neck cancer: A matched control study. Head & neck 35(8), 1096-1100.

Kumar, S., Kumar, S., Tiwari, S., Srivastava, S., Srivastava, M., Yadav, B.K., Kumar, S., Tran, T.T., Dewan, A.K., Mulchandani, A., 2015. Biofunctionalized nanostructured zirconia for biomedical application: a smart approach for oral cancer detection. Advanced Science 2(8).

Kumar, S., Sharma, J.G., Maji, S., Malhotra, B.D., 2016. Nanostructured zirconia decorated reduced graphene oxide based efficient biosensing platform for non-invasive oral cancer detection. Biosensors and Bioelectronics 78, 497-504.

Kumari, L., Zhang, T., Du, G., Li, W., Wang, Q., Datye, A., Wu, K., 2008. Thermal properties of CNT-Alumina nanocomposites. Composites Science and Technology 68(9), 2178-2183.

Laschi, S., Tombelli, S., Palchetti, I., Mascini, M., Marrazza, G., 2014. New affinity biosensors as diagnostic tools for tumour marker analysis. Sensors, pp. 19-23. Springer.

Le Coadou, C., Karst, N., Emieux, F., Sicardy, O., Montani, A., Bernard-Granger, G., Chevalier, J., Gremillard, L., Simonato, J.-P., 2015. Assessment of ultrathin yttria-stabilized zirconia foils for biomedical applications. Journal of Materials Science 50(18), 6197-6207.

Liang, L., Su, M., Li, L., Lan, F., Yang, G., Ge, S., Yu, J., Song, X., 2016. Aptamer-based fluorescent and visual biosensor for multiplexed monitoring of cancer cells in microfluidic paper-based analytical devices. Sensors and Actuators B: Chemical 229, 347-354.

Lingen, M.W., Kalmar, J.R., Karrison, T., Speight, P.M., 2008. Critical evaluation of diagnostic aids for the detection of oral cancer. Oral oncology 44(1), 10-22.

Liu, Y., Zhou, S., Tu, D., Chen, Z., Huang, M., Zhu, H., Ma, E., Chen, X., 2012. Amine-functionalized lanthanide-doped zirconia nanoparticles: optical spectroscopy, time-resolved fluorescence resonance energy transfer biodetection, and targeted imaging. Journal of the American Chemical Society 134(36), 15083-15090.

Low, K.P., Bhuvaneswari, R., Thong, P.S., Bunte, R.M., Soo, K.C., 2016. Novel delivery of Chlorin e6 using anti-EGFR antibody tagged virosomes for fluorescence diagnosis of oral cancer in a hamster cheek pouch model. European Journal of Pharmaceutical Sciences 83, 143-154.

Lughi, V., Sergo, V., 2010. Low temperature degradation-aging-of zirconia: A critical review of the relevant aspects in dentistry. Dental materials 26(8), 807-820.

Macwan, I., Patra, P., Khan, D.H., Singh, S., Aphale, A., Liu, J., Hingorani, M., 2016. A Novel Nano-biosensor for Colorectal Cancer Diagnostics by Detecting DNA Mismatch Repair Proteins.

Malhotra, B.D., Kumar, S., Pandey, C.M., 2016. Nanomaterials based biosensors for cancer biomarker detection. Journal of Physics: Conference Series, p. 012011. IOP Publishing.

Meda, L., Marra, G., Galfetti, L., Severini, F., De Luca, L., 2007. Nano-aluminum as energetic material for rocket propellants. Materials Science and Engineering: C 27(5), 1393-1396.

Mehrotra, R., Gupta, D.K., 2011. Exciting new advances in oral cancer diagnosis: avenues to early detection. Head & neck oncology 3(1), 1.

Menzies, G.E., Fox, H.R., Marnane, C., Pope, L., Prabhu, V., Winter, S., Derrick, A.V., Lewis, P.D., 2014. Fourier transform infrared for noninvasive optical diagnosis of oral, oropharyngeal, and laryngeal cancer. Translational Research 163(1), 19-26.

Mishra, S., Saadat, D., Kwon, O., Lee, Y., Choi, W.-S., Kim, J.-H., Yeo, W.-H., 2016. Recent advances in salivary cancer diagnostics enabled by biosensors and bioelectronics. Biosensors and Bioelectronics 81, 181-197.

Miyoshi, S., Akao, Y., Kuwata, N., Kawamura, J., Oyama, Y., Yagi, T., Yamaguchi, S., 2014. Low-Temperature Protonic Conduction Based on Surface Protonics: An Example of Nanostructured Yttria-Doped Zirconia. Chemistry of Materials 26(18), 5194-5200.

Moody, G., 2013. Confinement Effects on the Electronic and Optical Properties of Semiconductor Quantum Dots Revealed with Two-Dimensional Coherent Spectroscopy. Citeseer.

Muhamad12, I.I., Selvakumaran, S., Lazim, N.A.M., 2014. Designing Polymeric Nanoparticles for Targeted Drug Delivery System. Nanomedicine 287, 287.

Mukhopadhyay, A., Basu, B., 2013. Consolidation–microstructure–property relationships in bulk nanoceramics and ceramic nanocomposites: a review. International Materials Reviews.

Musil, J., 2012. Hard nanocomposite coatings: thermal stability, oxidation resistance and toughness. Surface and Coatings Technology 207, 50-65.

Nagler, R., Bahar, G., Shpitzer, T., Feinmesser, R., 2006. Concomitant analysis of salivary tumor markers—a new diagnostic tool for oral cancer. Clinical Cancer Research 12(13), 3979-3984.

Nikoleli, G.-P., Karapetis, S., Bratakou, S., Nikolelis, D.P., Tzamtzis, N., Psychoyios, V.N., Psaroudakis, N., 2016. Biosensors for Security and Bioterrorism: Definitions, History, Types of Agents, New Trends and Applications. Biosensors for Security and Bioterrorism Applications, pp. 1-13. Springer.

Noh, H.-S., Yoon, K.J., Kim, B.-K., Je, H.-J., Lee, H.-W., Lee, J.-H., Son, J.-W., 2014. The potential and challenges of thin-film electrolyte and nanostructured electrode for yttria-stabilized zirconia-base anode-supported solid oxide fuel cells. Journal of Power Sources 247, 105-111.

Palmero, P., Montanaro, L., Reveron, H., Chevalier, J., 2014. Surface coating of oxide powders: A new synthesis method to process biomedical grade nano-composites. Materials 7(7), 5012-5037.

Patton, L.L., Epstein, J.B., Kerr, A.R., 2008. Adjunctive techniques for oral cancer examination and lesion diagnosis: a systematic review of the literature. The Journal of the American Dental Association 139(7), 896-905.

Puchy, V., Hvizdos, P., Dusza, J., Kovac, F., Inam, F., Reece, M., 2013. Wear resistance of Al 2 O 3–CNT ceramic nanocomposites at room and high temperatures. Ceramics International 39(5), 5821-5826.

Rajaraman, P., Anderson, B.O., Basu, P., Belinson, J.L., D'Cruz, A., Dhillon, P.K., Gupta, P., Jawahar, T.S., Joshi, N., Kailash, U., 2015. Recommendations for screening and early detection of common cancers in India. The Lancet Oncology 16(7), e352-e361.

Rajkumar, K., Ramya, R., Nandhini, G., Rajashree, P., Ramesh Kumar, A., Nirmala Anandan, S., 2015. Salivary and serum level of CYFRA 21-1 in oral precancer and oral squamous cell carcinoma. Oral diseases 21(1), 90-96.

Reiner-Rozman, C., Kotlowski, C., Knoll, W., 2016. Electronic Biosensing with Functionalized rGO FETs. Biosensors 6(2), 17.

Ren, Y., Deng, H., Shen, W., Gao, Z., 2013. A highly sensitive and selective electrochemical biosensor for direct detection of microRNAs in serum. Analytical chemistry 85(9), 4784-4789.

Scherrer, B., Schlupp, M.V., Stender, D., Martynczuk, J., Grolig, J.G., Ma, H., Kocher, P., Lippert, T., Prestat, M., Gauckler, L.J., 2013. On proton conductivity in porous and dense yttria stabilized zirconia at low temperature. Advanced Functional Materials 23(15), 1957-1964.

Shao, Y., Wang, J., Wu, H., Liu, J., Aksay, I.A., Lin, Y., 2010. Graphene based electrochemical sensors and biosensors: a review. Electroanalysis 22(10), 1027-1036.

Shen, H., Zhang, L., Liu, M., Zhang, Z., 2012. Biomedical applications of graphene. Theranostics 2(3), 283-294.

Shin, S.I., Go, A., Kim, I.Y., Lee, J.M., Lee, Y., Hwang, S.-J., 2013. A beneficial role of exfoliated layered metal oxide nanosheets in optimizing the electrocatalytic activity and pore structure of Pt-reduced graphene oxide nanocomposites. Energy & Environmental Science 6(2), 608-617.

Shpitzer, T., Hamzany, Y., Bahar, G., Feinmesser, R., Savulescu, D., Borovoi, I., Gavish, M., Nagler, R., 2009. Salivary analysis of oral cancer biomarkers. British journal of cancer 101(7), 1194-1198.

Singh, A., Poshtiban, S., Evoy, S., 2013. Recent advances in bacteriophage based biosensors for food-borne pathogen detection. Sensors 13(2), 1763-1786.

Song, Y., Luo, Y., Zhu, C., Li, H., Du, D., Lin, Y., 2016. Recent advances in electrochemical biosensors based on graphene two-dimensional nanomaterials. Biosensors and Bioelectronics 76, 195-212.

Sorrentino, A., Gorrasi, G., Vittoria, V., 2007. Potential perspectives of bio-nanocomposites for food packaging applications. Trends in Food Science & Technology 18(2), 84-95.

Sponchia, G., Ambrosi, E., Rizzolio, F., Hadla, M., Del Tedesco, A., Spena, C.R., Toffoli, G., Riello, P., Benedetti, A., 2015. Biocompatible tailored zirconia mesoporous nanoparticles with high surface area for theranostic applications. Journal of Materials Chemistry B 3(36), 7300-7306.

Srivastava, M., Singh, J., Kuila, T., Layek, R.K., Kim, N.H., Lee, J.H., 2015. Recent advances in graphene and its metal-oxide hybrid nanostructures for lithium-ion batteries. Nanoscale 7(11), 4820-4868.

Sun, H., You, X., Deng, J., Chen, X., Yang, Z., Ren, J., Peng, H., 2014. Novel graphene/carbon nanotube composite fibers for efficient wire-shaped miniature energy devices. Advanced Materials 26(18), 2868-2873.

Teymourian, H., Salimi, A., Firoozi, S., Korani, A., Soltanian, S., 2014. One-pot hydrothermal synthesis of zirconium dioxide nanoparticles decorated reduced graphene oxide composite as high performance electrochemical sensing and biosensing platform. Electrochimica Acta 143, 196-206.

Tredici, I.G., Sebastiani, M., Massimi, F., Bemporad, E., Resmini, A., Merlati, G., Anselmi-Tamburini, U., 2016. Low temperature degradation resistant nanostructured yttria-stabilized zirconia for dental applications. Ceramics International 42(7), 8190-8197.

Walt, D.R., 2005. Miniature analytical methods for medical diagnostics. Science 308(5719), 217-219.

Wang, C., Cheng, L., Liu, Z., 2011. Drug delivery with upconversion nanoparticles for multi-functional targeted cancer cell imaging and therapy. Biomaterials 32(4), 1110-1120.

Wang, J., 2005. Nanomaterial-based electrochemical biosensors. Analyst 130(4), 421-426.

Wang, J., 2008. Electrochemical glucose biosensors. Chemical reviews 108(2), 814-825.

Wei, J., Xie, G., Zhou, Z., Shi, P., Qiu, Y., Zheng, X., Chen, T., Su, M., Zhao, A., Jia, W., 2011. Salivary metabolite signatures of oral cancer and leukoplakia. International journal of cancer 129(9), 2207-2217.

Wiklund, E.D., Gao, S., Hulf, T., Sibbritt, T., Nair, S., Costea, D.E., Villadsen, S.B., Bakholdt, V., Bramsen, J.B., Sørensen, J.A., 2011. MicroRNA alterations and associated aberrant DNA methylation patterns across multiple sample types in oral squamous cell carcinoma. PLoS One 6(11), e27840.

Wu, B., Zheng, N., 2013. Surface and interface control of noble metal nanocrystals for catalytic and electrocatalytic applications. Nano Today 8(2), 168-197.

Wu, H.-W., 2016. Label-Free and Antibody-Free Wideband Microwave Biosensor for Identifying the Cancer Cells. IEEE Transactions on Microwave Theory and Techniques 64(3), 982-990.

Wu, H.B., Chen, J.S., Hng, H.H., Lou, X.W.D., 2012. Nanostructured metal oxide-based materials as advanced anodes for lithium-ion batteries. Nanoscale 4(8), 2526-2542.

Xia, H., Wang, Y., Lin, J., Lu, L., 2012. Hydrothermal synthesis of MnO 2/CNT nanocomposite with a CNT core/porous MnO 2 sheath hierarchy architecture for supercapacitors. Nanoscale research letters 7(1), 1.

Xie, G.X., Chen, T.L., Qiu, Y.P., Shi, P., Zheng, X.J., Su, M.M., Zhao, A.H., Zhou, Z.T., Jia, W., 2012. Urine metabolite profiling offers potential early diagnosis of oral cancer. Metabolomics 8(2), 220-231.

Yang, T., Guo, X., Kong, Q., Yang, R., Li, Q., Jiao, K., 2013. Comparative studies on zirconia and graphene composites obtained by one-step and stepwise electrodeposition for deoxyribonucleic acid sensing. Analytica chimica acta 786, 29-33.

Zhang, C., Li, C.-J., Zhang, G., Ning, X.-J., Li, C.-X., Liao, H., Coddet, C., 2007. Ionic conductivity and its temperature dependence of atmospheric plasma-sprayed yttria stabilized zirconia electrolyte. Materials Science and Engineering: B 137(1), 24-30.

Zhang, W., Asiri, A.M., Liu, D., Du, D., Lin, Y., 2014. Nanomaterial-based biosensors for environmental and biological monitoring of organophosphorus pesticides and nerve agents. TrAC Trends in Analytical Chemistry 54, 1-10.

Zhao, X., Wei, C., Yang, L., Chou, M., 2004. Quantum confinement and electronic properties of silicon nanowires. Physical review letters 92(23), 236805.

Zhu, C., Yang, G., Li, H., Du, D., Lin, Y., 2014. Electrochemical sensors and biosensors based on nanomaterials and nanostructures. Analytical chemistry 87(1), 230-249.

Zygogianni, A.G., Kyrgias, G., Karakitsos, P., Psyrri, A., Kouvaris, J., Kelekis, N., Kouloulias, V., 2011. Oral squamous cell cancer: early detection and the role of alcohol and smoking. Head & neck oncology 3(1), 1.